DOKUZ EYLÜL UNIVERSITY

GRADUATE SCHOOL OF NATURAL AND APPLIED SCIENCES

DYNAMIC ANALYSIS OF PLANAR MANIPULATORS WITH LINEARLY TAPERED BEAMS

by

Mehmet DİRİLMİŞ

May, 2018

İZMİR

DYNAMIC ANALYSIS OF PLANAR MANIPULATORS WITH LINEARLY TAPERED BEAMS

A Thesis Submitted to the
Graduate School of Natural and Applied Sciences of Dokuz Eylül University In Partial Fulfillment of the Requirements for the Degree of Doctor of Philosophy in Mechanical Engineering, Machine Theory and Dynamics Program

by

Mehmet DİRİLMİŞ

May, 2018
İZMİR

Ph.D. THESIS EXAMINATION RESULT FORM

We have read the thesis entitled **"DYNAMIC ANALYSIS OF PLANAR MANIPULATORS WITH LINEARLY TAPERED BEAMS"** completed by **MEHMET DİRİLMİŞ** under supervision of **PROF.DR. HİRA KARAGÜLLE** and we certify that in our opinion it is fully adequate, in scope and in quality, as a thesis for the degree of Doctor of Philosophy.

Prof. Dr. Hira KARAGÜLLE

Supervisor

Prof. Dr. Murat KISA

Thesis Committee Member

Prof. Dr. Ramazan KARAKUZU

Thesis Committee Member

Prof. Dr. Hasan YILDIZ

Examining Committee Member

Assoc. Prof. Dr. Zekeriya GİRGİN

Examining Committee Member

Prof. Dr. Latif SALUM

Director

Graduate School of Natural and Applied Sciences

ACKNOWLEDGMENT

I would like to thank my supervisor Prof. Dr. Hira KARAGÜLLE for his valuable advice, continuous encouragement and support.

I would also like to thank Prof. Dr. Murat KISA, Prof. Dr. Ramazan KARAKUZU and Prof. Dr. Hasan ÖZTÜRK for the useful discussions and valuable advices.

I would like to thank Assist. Prof. Murat AKDAĞ and Assist. Prof. Şahin YAVUZ in BATÜL (Computer Aided Design-Analysis-Manufacturing Lab) for their helps.

Finally, I would like to thank my parents and my wife who have supported me since the beginning of my thesis works.

Mehmet DİRİLMİŞ

DYNAMIC ANALYSIS OF PLANAR MANIPULATORS WITH LINEARLY TAPERED BEAMS

ABSTRACT

In this thesis, two-link planar robot manipulator configurations with linearly tapered beams are considered. The manipulators have flexible joints and flexible links. The dynamic modeling of the studied manipulators for modal and transient analyses are done with MatLAB codes using the finite element theory. Also, experimental results are presented for the studied different manipulator systems. In the studies, the end point vibration signals are simulated by developing a MatLAB code based on the finite element theory and Newmark numerical integration. The mass and stiffness matrices are time dependent because the angular positions of the links change during the motion. Trapezoidal velocity profiles for the actuating motors are used. The time dependent inertia forces are calculated by using the rigid body dynamics. Residual vibrations that occur after the robot arms stop are minimized by setting of deceleration time values in the trapezoidal velocity profile as proposed. The root mean square (rms) acceleration values of the vibration signals after stopping are calculated. Many starting and stopping positions are examined. It is observed that simulation and experimental results are in good agreement. It is shown that by setting of the deceleration time as proposed, the residual vibration of a two-link manipulator with linearly tapered beams can be controlled.

Keywords: Two-link manipulator, tapered beams, non-uniform, flexible systems, finite elements analysis, modal analysis, transient analysis, vibration control

LİNEER DEĞİŞKEN KESİTLİ DÜZLEMSEL MANİPÜLATÖRLERİN DİNAMİK ANALİZİ

ÖZ

Bu tezde, esnek mafsal ve esnek kollara sahip lineer değişken kesitli iki kollu robot manipülatörler incelenmiştir. İncelenen manipülatörlerin dinamik analizleri için sonlu elemanlar yöntemine uygun olarak direct ve exact formülasyon yöntemleri ile matematiksel modelleme yapılmıştır. İncelenen manipülatörlerin sonlu elemanlar teorisine göre dinamik modellemesi yapılarak MatLAB programlama kodları ile modal analiz ve geçiş rejimi analizleri için parametrik esaslı programlar geliştirilmiştir. Sistemlerin dinamik analizi için elde edilen diferansiyel denklemlerin çözümünde Newmark nümerik integrasyon yöntemi kullanılmıştır. Bu program ile uç noktanın titreşim sinyalleri elde edilmiştir. İncelenen farklı manipülatör sistemleri için prototipler üretilerek deneysel sonuçlar elde edilmiştir. İki kollu sistemlerde, hareket boyunca kolların açısal pozisyonları değiştiği için kütle ve rijitlik matrisleri de zamana göre değişmektedir. Motorları sürmek için trapez hız profilleri kullanılmıştır. Rijit cisim dinamiği kullanılarak zamana bağlı atalet kuvvetleri hesaplanmıştır. Hız profilindeki durma zamanı değerinin manipülatör sisteminin birinci doğal frekansı ile ilişkilendirilip ayarlanmasıyla artık titreşimlerin azaldığı gösterilmiştir. İki kollu değişken kesitli bir robot manipülatörde durduktan sonra oluşan artık titreşimlerin, trapez hız profilindeki durma zamanı değerlerinin bu çalışmada önerildiği gibi ayarlanmasıyla azaldığı deneysel ve nümerik olarak gösterilmiştir. Çeşitli başlama ve durma pozisyonları incelenmiştir. Deney ve simülasyon sonuçlarının birbirleriyle uyumlu olduğu görülmüştür.

Anahtar kelimeler: İki kollu manipülatör, konik kirişler, değişken kesit, esnek sistemler, sonlu elemanlar analizi, modal analiz, geçiş rejimi analizi, titreşim kontrolü

CONTENTS

Page

LIST OF FIGURES

Page

LIST OF TABLES

Page

CHAPTER ONE
INTRODUCTION

1.1 Introduction

Beams are one of the common types of structural components and they are basically categorized according to their geometric configuration as uniform and non-uniform beams. These structural elements are commonly used in various engineering applications, such as, robot manipulator links, wind turbines, helicopter rotor blades, and space and marine structures. Non-uniform tapered beams with varying cross-section provide a better distribution of mass and strength than uniform beams. The advantages of these tapered beams are structural efficiency, high stiffness/weight ratio and offering an additional design parameter. Accordingly, the tapered beams can meet special functional requirements in structural design, especially in robotics, and other advanced engineering applications. Therefore, estimate and determination of dynamic behavior of these structures have been an area of great interest among researchers.

Vibrations caused after the end of motion are known as residual vibrations. The residual vibrations also affect the correctness and settling time at the end point of manipulator. Flexibility of robot manipulators depends on the parameters such as weight, dimension, payload and speed of manipulators. The effect of flexibility in manipulators is observed as vibrations both during the motion and after the motion. The performance of such manipulators or repeatability decreases in high speed engineering applications. Suppressing residual vibrations are important and it is possible to surpress residual vibration by applying different control strategies such as passive or active. In this thesis, residual vibration control presented by passive control (open loop) strategies with the settings of deceleration time parameters.

Flexible manipulators are used in robotic systems design, flexible gyroscopes, and multibody systems. A simple and accurate dynamic model is necessary for determination of the dynamic behavior of the flexible multibody systems. In this

thesis, a dynamic model based MatLAB code with finite element procedures was developed for the two-link planar manipulator with linearly tapered beams. Also, the studied manipulator systems had flexible joints and flexible links.

1.2 Literature Review

Analyzing the nonlinear vibration of beams is one of the important issues in structural engineering. Applications such as high-rise buildings, long-span bridges, and aerospace vehicles have necessitated the study of their dynamic behavior at large amplitudes. Many researchers have studied tapered beams, which are very important for the design of many engineering structures (Bayat et al., 2011).

The mathematical models of manipulators can be constructed by the finite element method or analytical methods. The first step to the dynamic analyses is establish the mathematical models of manipulator systems. Control of multi-link flexible manipulators reviewed in reference (Benosman & LeVey, 2004) by considering the control objectives of end-effector position and trajectory tracking. The governing differential equations of dynamic systems can be solved by using numerical methods (Fung, 1997; Owren & Simonsen, 1995; Zhang et al., 1999) or commercial engineering programs (Karagulle & Malgaca, 2004). Dynamic analysis of flexible manipulators reviewed in detail by classifying single-link, two-link, and multi-link manipulators (Dwivedy & Eberhard, 2006).

Active (closed loop) or passive (open loop) control techniques can be applied to suppress their residual vibrations of flexible robot manipulators. A passive control technique can be perform with motion commands without using any additional hardware while an active control technique requires a new actuator, a sensor and a control system. A passive control can be performed as open loop while an active control can be achieved as closed loop. The closed loop control of flexible manipulator with both single-link and two-link has been studied in the literature (Shin & Choi, 2001; Gurses et al., 2009, Mirzaee et al., 2010). Most of these studies

used piezoelectric actuators to reduce the residual vibration of flexible robot manipulators.

Some studies are related to designing and selecting appropriate trajectories to reduce residual vibrations. Park (2004) studied control of residual vibration of two-link manipulator by designing and optimizing a path under torque constraints. Abe (2009) also proposed an optimal trajectory planning for residual suppression of a two-link rigid-flexible link by using the Lagrangian approach and the assumed modes method. Green & Sasiadek (2004) presented control methods such as LQR and fuzzy logic for end point tracking of a trajectory by a two-link manipulator.

The passive control of single-link flexible manipulators was studied in the literature extensively (Ankarali & Diken, 1997; Mimmi & Pennacchi, 2001; Shan et al., 2005; Shin & Brennan, 2008). Residual vibrations are suppressed or eliminated by changing motion inputs with an open loop control. However, there are limited studies regarding the passive control of two-link or multi-link manipulators. Ozer & Semercigil (2008) demonstrated the effectiveness of the variable stiffness control technique on a two-link manipulator with passive components to implement control action.

In the references (Ankaralı & Diken, 1997; Shin & Brennan, 2008), it was shown that by selecting an appropriate deceleration time, the residual vibrations of single-link manipulators could be controlled. Ankaralı & Diken (1997) solved the transient vibration problem of a single elastic link, which was modeled by using Euler-Bernoulli beam theory and mode summation techniques. Karagulle et al. (2015) have studied on the vibration control of two-link flexible manipulator with uniform cross-section beams.

In this study, the approach as residual vibration control by setting of deceleration time parameters has been extended to a two-link tapered flexible manipulator to control its residual vibrations. Theoretical results based on the finite element method

were obtained by defining trapezoidal motion inputs for various end point positions of the manipulator.

1.3 Scobe of the Thesis

Dynamic analysis of moving flexible arm connected to each joints is required for manipulator design and its use. A simple and accurate dynamic model of the flexible multibody systems such as flexible manipulator is important for design and its use.

In the study, a dynamic analysis program with parametric variables based MatLAB code was developed with finite element procedures for flexible tapered manipulator system. The simulation results of the dynamic responses of the manipulator systems obtained from developed dynamic analysis program for different motion Cases. Experimental prototypes of the flexible tapered manipulator system were produced. The simulation results were verified and compared with the experimental results.

The dynamic analyses carried out for various Case studies of two-link flexible manipulators with linearly tapered beams. The setting of deceleration time method was proposed for the residual vibration control of the two-link tapered manipulator systems. Modal analysis and transient analysis results were obtained as simulation and experimental.

1.4 Organization of the Thesis

The thesis study contains seven chapters and appendices.

Chapter 1 presents the important of using of tapered beams and the advantages of flexible manipulators, literature survey, and organization of the thesis.

Chapter 2 presents fundamentals of finite element modeling of the tapered manipulator system with flexible joints and flexible links. The direct formulation

method with the finite element used to obtaining mathematics model of the system. The finite element dynamics model of the system was developed by MatLAB codes. The parametric program codes attached to thesis appendixes.

Chapter 3 presents the finite element model with exact formulation of the two-link flexible manipulator with linearly tapered beams. In this section, the element stiffness and mass matrix obtained with exact formulation based finite element method. The finite element model was developed by MatLAB codes. The program codes are shown in thesis appendixes.

Chapter 4 presents the experimental vibration analyses of the two-link flexible manipulator systems. The experimental setup and the measurement systems are shown and the modal and transient analyses results are presented.

Chapter 5 presents the experimental and the simulation results and discussions. The Case studies are presented for System-1-varying-AL, System-2-equivalent-uniform-AL and System-3-varying-AL. The modal, transient analyses and vibration control cases are presented in this chapter.

Finally, the conclusions are presented in the chapter 6. Moreover, the suggestions for the future works are presented in this chapter.

CHAPTER TWO
FINITE ELEMENT MODELING OF TWO-LINK MANIPULATORS WITH LINEARLY TAPERED BEAMS (MODEL-I)

2.1 Introduction

The theoretical model of the flexible two-link manipulator with linearly tapered beams for this study is shown in Figure 2.1. There are revolute joints at O and A. The Member-1 is fixed frame, OA_1-beam is Member-2 (tapered arm 1), AB-beam is Member-3 (tapered arm 2). The Member-2 is actuated by Motor-2 at point O, and the Member-3 is actuated by Motor-3 at point A. The point O is the global origin and x, y, z are the global Cartesian coordinates. The instantaneous position of the manipulator is defined by θ_2 and θ_3. The mass of the first servo motor is on the frame (Member-1) at point O. The mass of the second servo motor is on Member-2 at point A. The B is the end point of the two-link tapered manipulator. There is a payload mass on Member-3 at point B. θ_2 is the instantaneous angular positions of Member-2 and θ_3 is the instantaneous angular positions of Member-3. L_2=OA, L_3=AB.

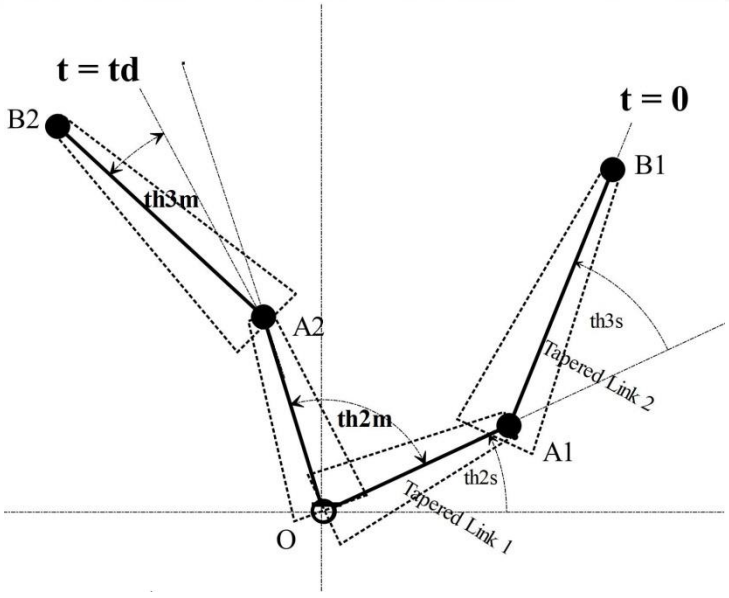

Figure 2.1 The theoretical model of the studied two-link manipulator with linearly tapered beams

The studied two-link manipulator with linearly tapered beams is shown in Figure 2.2.a and the stepped beam model with FEM direct formulation of the manipulator is shown in Figure 2.2.b.

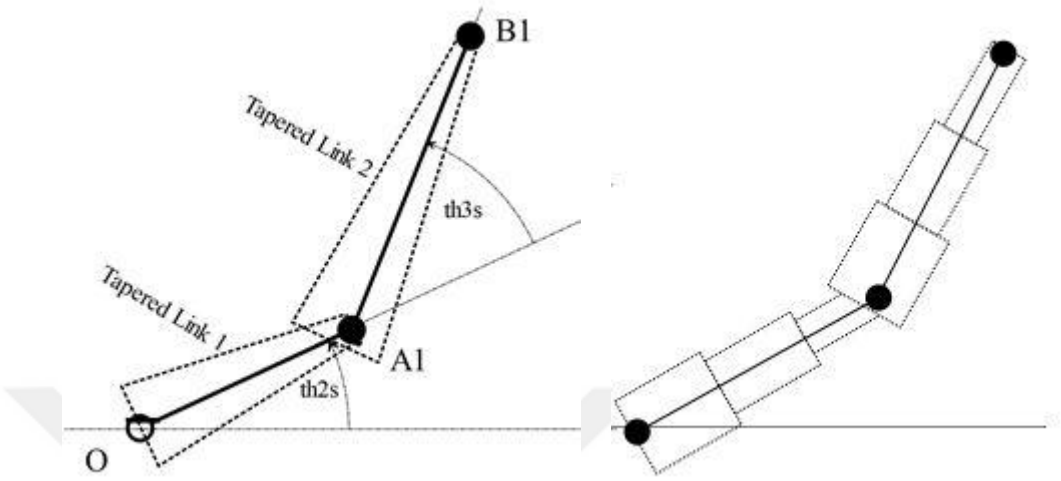

a) The studied two-link manipulator with linearly tapered beams

b) The stepped beam model with FEM direct formulation of the manipulator

Figure 2.2 Two-link tapered flexible manipulator (a, b)

The finite elements and node numbers of the two-link manipulator system are shown in Figure 2.3. All nodes have three degree of freedom except node-2 and node-6 for the demonstration in the picture. There is one degree of freedom at Node-2 and node-6 in z direction as rotation due to torsional stiffness of flexible joint. In the representation at the figure, there are 7 nodes and 6 finite elements, and 2 nodes due to flexible joints. The total degree of freedom is (7*3)+1+1=23. The first node is fixed and the 3 dof are zero. The second node has only torsional stiffness due to joint flexibility of motor in z direction as rotation.

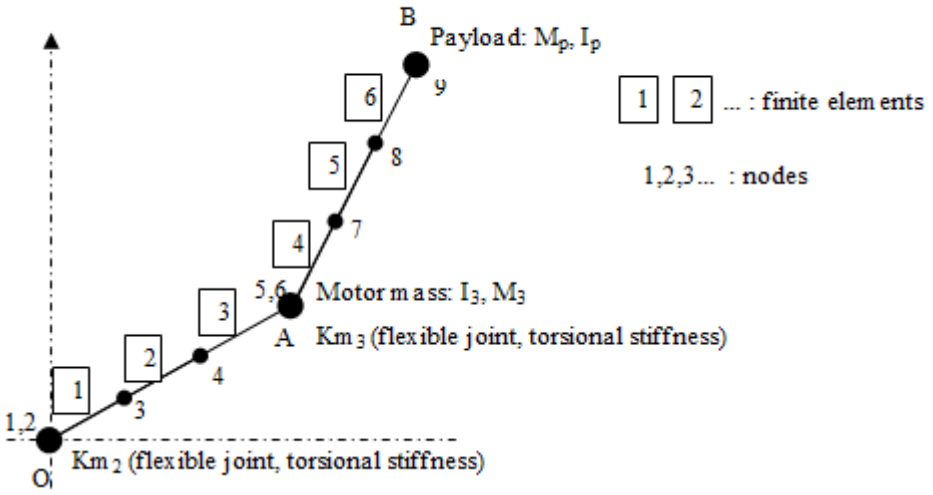

Figure 2.3 The finite elements and nodes of the two-link manipulator

The finite elements properties and the identification numbers for the model-1 of the two-link manipulator system are shown in Table 2.1.

Table 2.1 The finite elements and the identification numbers for the model-1 of the system

The finite element		On Member	FE Nodes	Length	Angle	Identification numbers for displacements at nodes
	1	2	2,3	L_2/n_{e2}	θ_2	21,22,1 -- 2,3,4
	2	2	3,4	L_2/n_{e2}	θ_2	2,3,4 -- 5,6,7
	3	2	4,5	L_2/n_{e2}	θ_2	5,6,7 -- 8,9,10
	4	3	6,7	L_3/n_{e3}	θ_3	8,9,11 -- 12,13,14
	5	3	7,8	L_3/n_{e3}	θ_3	12,13,14 -- 15,16,17
	6	3	8,9	L_3/n_{e3}	θ_3	15,16,17 -- 18,19,20

2.2 Finite Element Modeling with Direct Formulation

A tapered link is shown in Figure 2.4. The link has varying cross-section area. Direct formulation for finite element model was used.

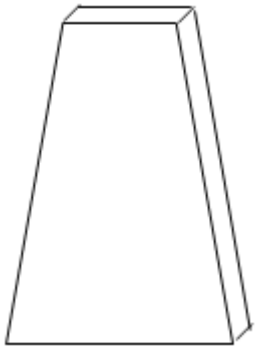

Figure 2.4 A tapered link

The tapered link can be modeled as a stepped beam with each region having a uniform cross-section. A sample model has 5 nodes and 4 finite elements as shown in Figure 2.5. This is done by dividing the tapered link into four regions. The average cross-sectional area within each region is evaluated and then used to define an element with uniform cross-section.

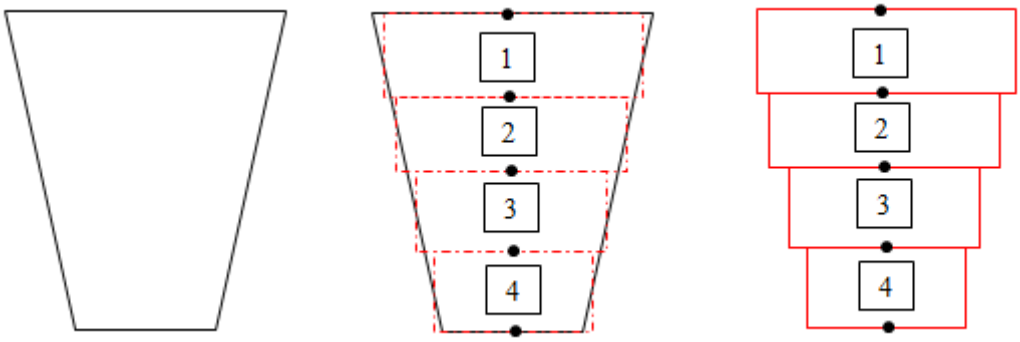

a) A tapered link

b) The average cross-sectional areas

c) The nodes and finite elements for a tapered link

Figure 2.5 Finite element modeling of a tapered link with direct formulation

The four beam finite elements and the five nodes are shown in Figure 2.6. In the finite element model, every element connects to two nodes. All nodes has three degree of freedom.

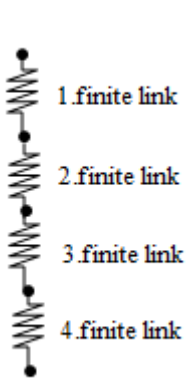

a) The finite elements

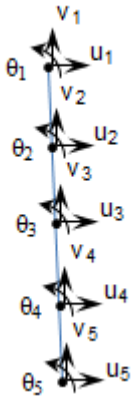

b) Degree of freedoms of nodes

Figure 2.6 The finite elements of the tapered beam

2.2.1 The Obtaining Element Stiffness Matrix

A general straight beam element with uniform cross section is shown in Figure 2.7. The element has constant moment of inertia of the cross-sectional area I, modulus of elasticity E, and length L. The element is assumed to have three degrees of freedom at each node: an axial deflection "u", a transverse deflection "v" and an angle of rotation θ or $\left(\frac{\partial v}{\partial x}\right)$. The element is capable of carrying axial forces, transverse forces and moments.

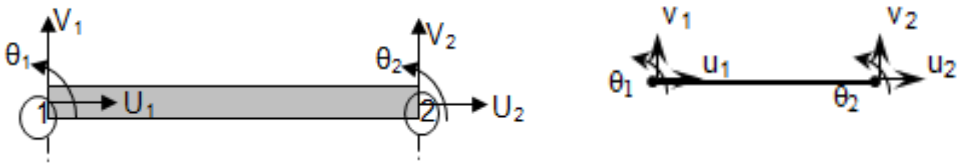

Figure 2.7 A general beam element with axial displacement

A frame element has both the properties of a truss element and a beam element. The element matrices for a frame element can be calculated by combining element matrices for truss and beam elements. The truss element has only one degree of freedom at each node (axial deformation), and the beam element has two degrees of freedom at each node (transverse deformation and rotation).

The assumed shape functions can be obtained by using a linear interpolation model for axial displacement and a cubic model for transverse displacement.

$$u(x) = \left(1 - \frac{x}{L}\right) u_1 + \frac{x}{L} u_2 \tag{2.1}$$

$$v(x) = c_0 + c_1 x + c_2 x^2 + c_3 x^3 \tag{2.2}$$

From the assumption for Euler-Bernoulli beam, slope is computed from Eq.(2).

$$\theta(x) = \frac{\partial v}{\partial x} = c_1 + 2c_2 x + 3c_3 x^2 \tag{2.3}$$

Evaluation of deflection and slope at both nodes yields,

$$\begin{aligned} v(0) &= c_0 = v_1 \\ \theta(0) &= c_1 = \theta_1 \\ v(L) &= c_0 + c_1 L + c_2 L^2 + c_3 L^3 = v_2 \\ \theta(L) &= c_1 + 2c_2 L + 3c_3 L^2 = \theta_2 \end{aligned} \tag{2.4}$$

Solving Eg. (2.4) for c_i in terms of nodal variables v_i and θ_i and substituting the results into Eg. (2.2) give

$$v(x) = H_1(x)v_1 + H_2(x)\theta_1 + H_3(x)v_2 + H_4(x)\theta_2 \tag{2.5}$$

Where,

$$H_1(x) = 1 - \frac{3x^2}{L^2} + \frac{2x^3}{L^3}$$

$$H_2(x) = x - \frac{2x^2}{L} + \frac{x^3}{L^2}$$

$$H_3(x) = \frac{3x^2}{L^2} - \frac{2x^3}{L^3} \tag{2.6}$$

$$H_4(x) = -\frac{x^2}{L} + \frac{x^3}{L^2}$$

The potential and the kinetic energies are shown in below for axial deformations.

$$V = \frac{1}{2}\int_0^L AE\left(\frac{\partial u}{\partial x}\right)^2 dx \qquad T = \frac{1}{2}\int_0^L \rho A\left(\frac{\partial u}{\partial t}\right)^2 dx \tag{2.7}$$

For axial loading, the stiffness matrix is,

$$k = \frac{AE}{L}\begin{bmatrix} 1 & -1 \\ -1 & 1 \end{bmatrix} \tag{2.8}$$

The potential and the kinetic energies are shown in below for transverse deformations.

$$V = \frac{1}{2}\int_0^L EI\left(\frac{\partial^2 v}{\partial x^2}\right)^2 dx \qquad T = \frac{1}{2}\int_0^L \rho A\left(\frac{\partial v}{\partial t}\right)^2 dx \tag{2.9}$$

The following stiffness matrix for the combined bending and axial load can be written by superimposing the axial stiffness terms over the bending stiffness for a general 2-D beam element,

$$K = \begin{bmatrix} \frac{AE}{L} & 0 & 0 & -\frac{AE}{L} & 0 & 0 \\ 0 & \frac{12EI}{L^3} & \frac{6EI}{L^2} & 0 & \frac{-12EI}{L^3} & \frac{6EI}{L^2} \\ 0 & \frac{6EI}{L^2} & \frac{4EI}{L} & 0 & \frac{-6EI}{L^2} & \frac{2EI}{L} \\ -\frac{AE}{L} & 0 & 0 & \frac{AE}{L} & 0 & 0 \\ 0 & \frac{-12EI}{L^3} & \frac{-6EI}{L^2} & 0 & \frac{12EI}{L^3} & \frac{-6EI}{L^2} \\ 0 & \frac{6EI}{L^2} & \frac{2EI}{L} & 0 & \frac{-6EI}{L^2} & \frac{4EI}{L} \end{bmatrix} \quad (2.10)$$

2.2.2 The Obtaining Element Mass Matrix

The mass matrix in local coordinates can be obtained by combining the resulting axial and transverse mass matrix by the same procedures. The obtained mass matrix for a finite element beam is shown below,

$$M = \frac{\rho AL}{420}\begin{bmatrix} 140 & 0 & 0 & 70 & 0 & 0 \\ 0 & 156 & 22L & 0 & 54 & -13L \\ 0 & 22L & 4L^2 & 0 & 13L & -3L^2 \\ 70 & 0 & 0 & 140 & 0 & 0 \\ 0 & 54 & 13L & 0 & 156 & -22L \\ 0 & -13L & -3L^2 & 0 & -22L & 4L^2 \end{bmatrix} \quad (2.11)$$

2.2.3 The Global Element Matrix

The local and global coordinate systems are shown in Figure 2.8. Transformations between local and global displacement can be written as

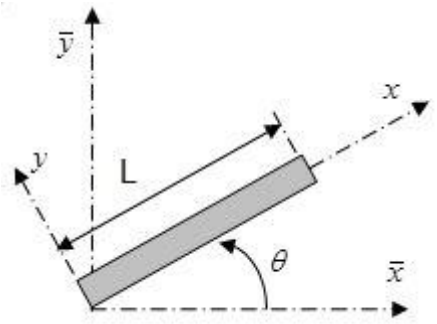

Figure 2.8 The local and global coordinate system

$$T = \begin{bmatrix} c & s & 0 & 0 & 0 & 0 \\ -s & c & 0 & 0 & 0 & 0 \\ 0 & 0 & 1 & 0 & 0 & 0 \\ 0 & 0 & 0 & c & s & 0 \\ 0 & 0 & 0 & -s & c & 0 \\ 0 & 0 & 0 & 0 & 0 & 1 \end{bmatrix} \tag{2.12}$$

$$c = \cos(\theta)$$
$$s = \sin(\theta) \tag{2.13}$$

$$\overline{K} = T^T.K.T$$
$$\overline{M} = T^T.M.T \tag{2.14}$$

Where, $\overline{k}$ is global stiffness matrix of an element, $\overline{m}$ is global mass matrix of an element, T is transformation matrix and T^T is transpose of the transformation matrix.

2.3 The Equation of Motion

The mathematical model of the system is obtained as,

$$m\ddot{d} + cd + k\dot{d} = f \tag{2.15}$$

2.4 The Rayleigh Damping

The Rayleigh damping is given by (Thomson & Dahleh, 1988).

$$c_s = \alpha.m_s + \beta.k_s \tag{2.16}$$

where, α and β are damping coefficients.

2.5 The Motion Parameters

The studied two-link manipulator systems moves from a starting position (OA_1B_1) at t=0 to an end position (OA_2B_2) at $t=t_m$. Where, t is time and t_m is the motion time.

The motors follow the trapezoidal velocity profile given in Figure 2.9. The motion control units which produce pulses according to the velocity profile. The area under the velocity curve gives the corresponding motor rotations, ϕ_{2m} and ϕ_{3m}.

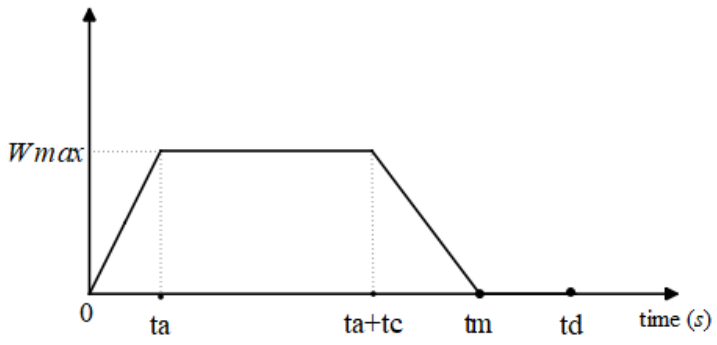

Figure 2.9 Trapezoidal velocity profile

The accelerations of the mid-points of the FE's are calculated to consider the distributed inertia forces. The rigid body kinematics is considered for the calculation. Let L_{nm} be the distance of a mid-point on Member-2 from Point-O. Then the position vector of the mid-point is written with complex numbers as $R_{nm} = L_{nm}e^{i\theta_2}$, where $i = \sqrt{-1}$. The real part of R_{nm} is the x component and the imaginary part is the y component. The second derivative of R_{nm} gives the acceleration as;

$$\mathrm{a}_{nm} = (i\dot{\theta}_2 - \ddot{\theta}_2^2)L_{nm}e^{i\theta_2} \tag{2.17}$$

Let L_{nm} be the distance of a mid-point on Member-3 from Point-B. Then the position vector of the mid-point is written with complex numbers as $\mathrm{R}_{nm} = L_2 e^{i\theta_2} + L_{nm}e^{i\theta_3}$. Then, $\mathrm{a}_{nm} = (i\dot{\theta}_2 - \ddot{\theta}_2^2)L_{OB}e^{i\theta_2} + (i\dot{\theta}_3 - \ddot{\theta}_3^2)L_{OB}e^{i\theta_3}$. a_{nmx}, and a_{nmy} are the x and y components of $\mathbf{a}_{nm}$, respectively.

Considering the velocity profile of motors, the following equations can be obtained.

$$\omega_{02} = \frac{\varphi_{2m}}{(0.5t_{acc} + t_{con} + 0.5t_{dec})} \tag{2.18}$$

$$\omega_{03} = \frac{\varphi_{3m}}{(0.5t_{acc} + t_{con} + 0.5t_{dec})} \tag{2.19}$$

Table 2.2 Trapezoidal velocity profile parameters

Time interval	Angular velocity	Angular displacement	Angular acceleration
$0 \le t < t_a$	$\omega = \omega_0 \dfrac{t}{t_d}$	$\theta = \dfrac{\omega_o t^2}{2t_a}$	$a = a_o$
$t_a \le t \le t_d - t_a$	$\omega = \omega_0$	$\theta = \dfrac{\omega_o t_a}{2} + \omega_o(t - t_a)$	$a = 0$
$t_d - t_a < t < t_d$	$\omega = \dfrac{\omega_o(t_d - t)}{t_a}$	$\theta = \theta_m - \dfrac{\omega_o(t_d - t)^2}{2t_a}$	$a = -a_o$
$t = t_d$	$\omega = 0$	$\theta = \theta_m$	$a = 0$

The angular displacement curve for trapezoidal motion profile is shown in Figure 2.10.

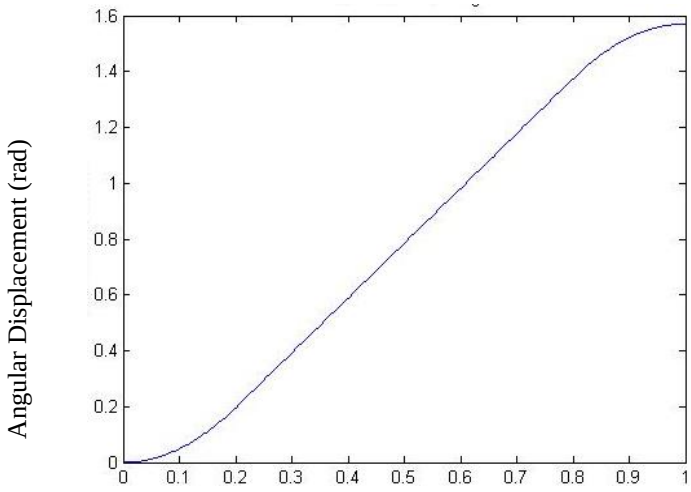

Figure 2.10 The displacement curve

The angular velocity curve for trapezoidal motion profile is shown in Figure 2.11.

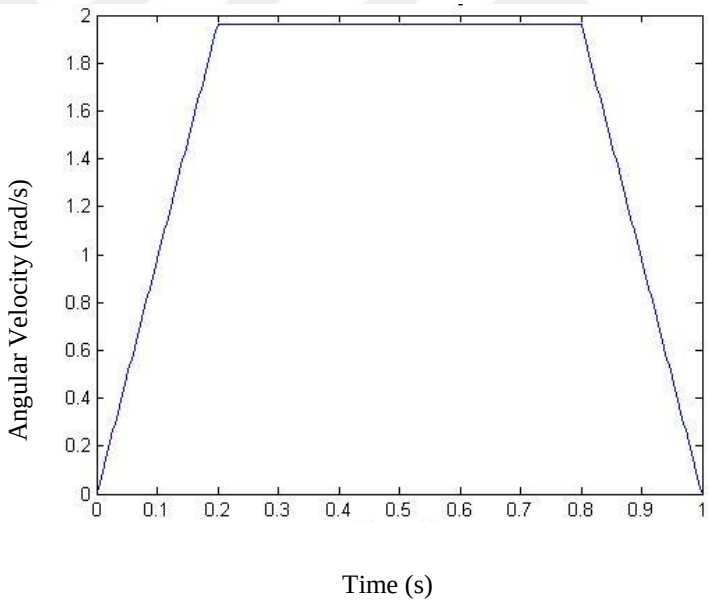

Figure 2.11 The velocity curve

The angular acceleration curve for trapezoidal motion profile is shown in Figure 2.12.

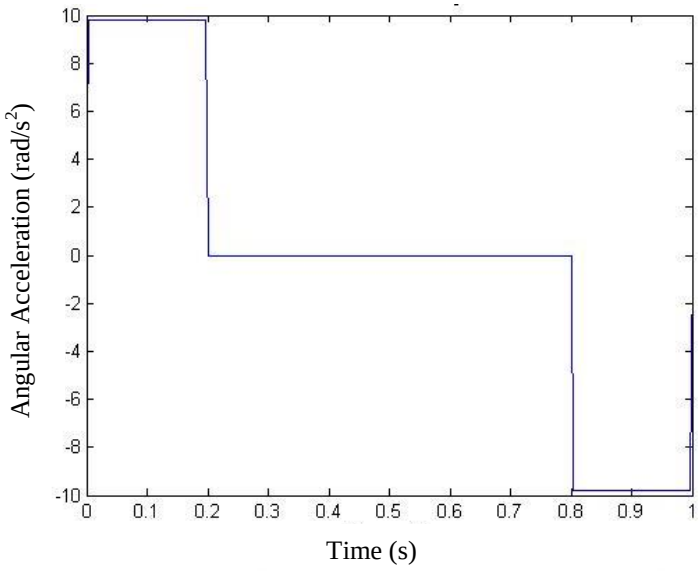

Figure 2.12 The acceleration curve

2.6 The Distributed Inertia Forces

The distributed inertia forces for the uniform cross-section and rectangular beam are given in Figure 2.13. Where q_{nx}, and q_{ny} is the distributed forces for FE-n. The forces can be written as follows;

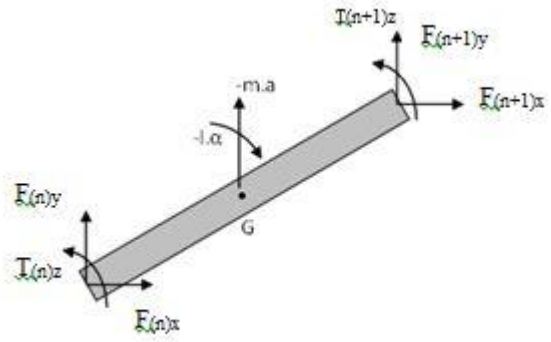

$$q_{nx} = -(\rho_n A_n h_n) a_{nmx}$$

$$q_{ny} = -(\rho_n A_n h_n)(a_{nmy})$$

Figure 2.13 The distributed forces for a finite element

For example, the nodal forces for Node-6 are formed due to the distributed forces for FE-3 and FE-4. So, the following equations can be written for the elements of the nodal force vector, f_s, corresponding to Node-6.

$\mathbf{f}_s(9,1)=q_{3x}h_3/2+ q_{4x}h_4/2,$

$\mathbf{f}_s(10,1)=q_{3y}h_3/2+ q_{4y}h_4/2,$

$\mathbf{f}_s(11,1)=q_{3y}h_3^2/12+ q_{4x}h_4^2/12.$

2.7 The Vibration Signals

The vibration of the receiving point located at a distance of d_{sensor} from the end-point, B, is analyzed. The vibration direction perpendicular to the line-AB in the x-y plane (motion plane) is considered. Let the displacement of the receiving point in the vibration direction be d_R. The second derivative of d_R is the acceleration signal and denoted by a_R. The gravity is in the z direction, and thus is not included.

2.8 The Modal Analysis

The following eigenvalue equation is solved for the modal analysis.

$$|-\omega^2 m_s + k_s| = 0 \tag{2.20}$$

The values of ω are the un-damped natural frequencies of the system. $\omega_1 T_1=2\pi$, where T_1 is the period corresponding the first natural frequency in seconds. $f_1=1/T_1$ is the first natural frequency in Hz. $T_{1h}=0{,}5.T_1$, and this value will be used to define t_{acc}, t_{con}, or t_{dec} below.

It is noted that the angles θ_2 and θ_3 change during the motion of the two-link system, and thus the transformation matrices, T_s, change for the FE's. So, the matrices, m_s, c_s and k_s, change; and thus the natural frequencies change depending on the position of the system.

2.9 The Transient Analysis by Newmark Method

The Newmark method (Newmark, 1959) was used for the transient analysis. A time step, Δt, was chosen for the solution as $\Delta t < T_{max}/20$. Where T_{max} is the period for the highest natural frequency considered.

The Newmark solution is given as

$$[a_0 m_{n+1} + a_1 c_{n+1} + k]d_{n+1} = f_n + m_n[a_0 d_n + a_2 \dot{d}_n + a_3 \ddot{d}_n] + c_n[a_1 d_n + a_4 \dot{d}_n + a_5 \ddot{d}_n]$$

$$\ddot{d}_{n+1} = a_0[d_{n+1} - d_n] - a_2 \dot{d}_n - a_3 \ddot{d}_n$$

$$\dot{d}_{n+1} = \dot{d}_n + a_6 \ddot{d}_n + a_7 \ddot{d}_{n+1}$$

$$a_0 = \frac{1}{\alpha \Delta t^2},\ a_1 = \frac{\delta}{\alpha \Delta t},\ a_2 = \frac{1}{\alpha \Delta t},$$

$$a_3 = \frac{1}{2\alpha} - 1,\ a_4 = \frac{\delta}{\alpha} - 1,\ a_5 = \frac{\Delta t}{2}\left(\frac{\delta}{\alpha} - 2\right),$$

$$a_6 = \Delta t(1 - \delta),\ a_7 = \delta \Delta t,$$

$$\alpha = \frac{1}{4}(1 + \gamma)^2,\ \delta = \frac{1}{2} + \gamma$$

Where, γ is the amplitude decay factor.

CHAPTER THREE
FINITE ELEMENT MODELING OF TWO-LINK MANIPULATORS WITH LINEARLY TAPERED BEAMS (MODEL-II)

3.1 Introduction

In the chapter, the exact stiffness and mass matrices were obtained for variable cross-sectional beam elements with two nodes and three degrees of freedom at each node. In the section, the exact formulation based finite element method was used for obtaining mathematical model of the system. A simulation program was developed by MatLAB based codes for the dynamics and vibration analysis of a two-link robot manipulator with flexible joints and variable cross-sectional flexible links. The flexible links had linearly tapered beams. Simulation results were obtained by using a developed MatLAB codes based on the finite element theory. The Newmark numerical solution method is used to solve the mathematical model which consisted of time dependent mass, stiffness and force matrices.

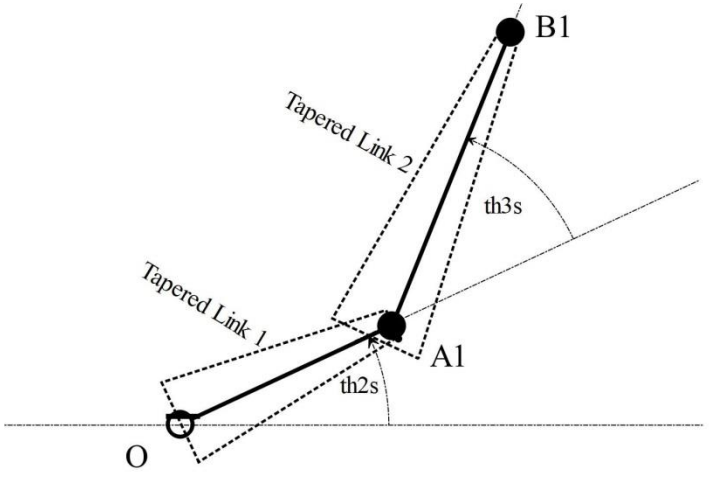

Figure 3.1 The theoretical model of the two-link manipulator with linearly tapered beams

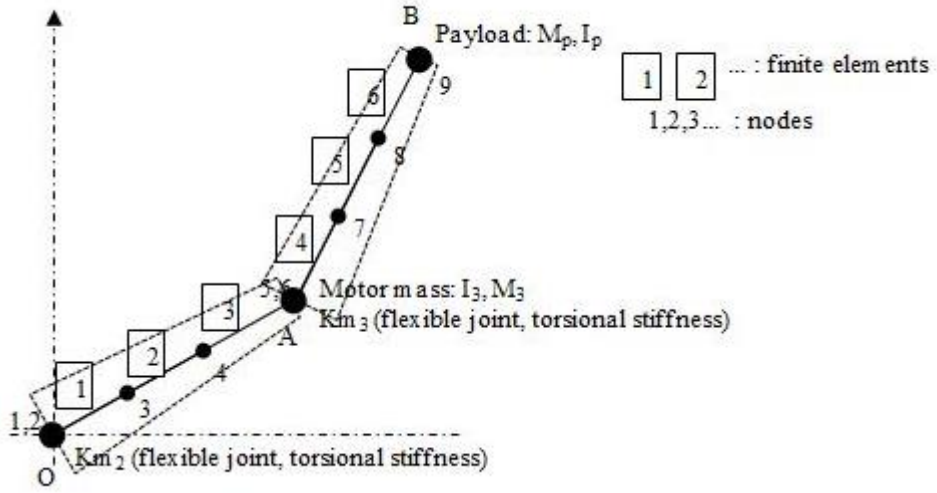

Figure 3.2 Exact model of two-link manipulator with linearly tapered beam

Table 3.1 The finite elements for model-2

The finite element		On Member	FE Nodes	Length	Angle	Identification numbers for displacements at nodes
	1	2	2,3	L_2/n_{e2}	θ_2	21,22,1-2,3,4
	2	2	3,4	L_2/n_{e2}	θ_2	2,3,4-5,6,7
	3	2	4,5	L_2/n_{e2}	θ_2	5,6,7-8,9,10
	4	3	6,7	L_3/n_{e3}	θ_3	8,9,11-12,13,14
	5	3	7,8	L_3/n_{e3}	θ_3	12,13,14-15,16,17
	6	3	8,9	L_3/n_{e3}	θ_3	15,16,17-18,19,20

In the section, the exact stiffness matrix was obtained for a linearly varying tapered beam which has two nodes and three degrees of freedom at each node.

3.2 Obtaining the Element Siffness Matrix for a Varying Cross-section

A variable cross-sectional tapered beam is shown in Figure 3.3. There are three degrees of freedom (u, v, θ) at each node. One element has 6 degrees of freedom in

total because each element has two nodes. Therefore, the stiffness matrix has an element is 6x6, the degrees of freedom vector is 6x1, and the external load vector is 6x1 size.

The stiffness matrix of a beam with variable cross section was obtained by appropriately combining the stiffness matrices which obtained for bending and axial deformation of the beam.

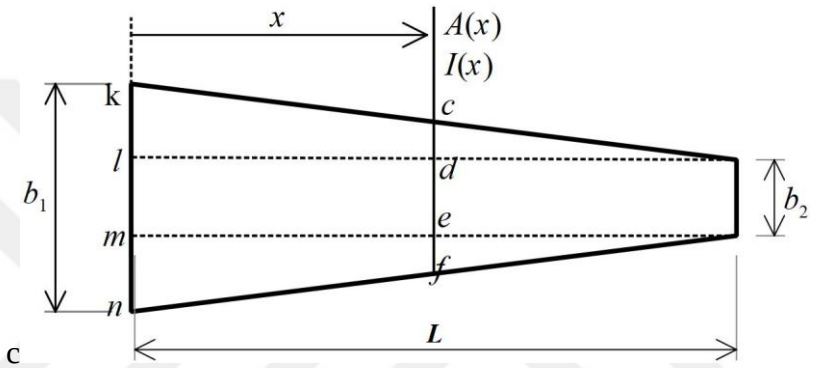

Figure 3.3 The considered beam with varying cross-section

$$b(x) = |cf|$$

$$|kl| = \frac{b_1 - b_2}{2}$$

$$\frac{|kl|}{L} = \frac{|cd|}{L-x} \Rightarrow |cd| = \frac{b_1 - b_2}{2} * \frac{L-x}{L} \tag{3.1}$$

$$|cf| = 2 * |cd| + b_2 \Rightarrow b(x) = b_2 + (b_1 - b_2).\left(1 - \frac{x}{L}\right)$$

$$b(x) = b_2 + (b_1 - b_2) * (1 - \frac{x}{L})$$

$$b(x) = b_2 + b_1 - b_2 - b_1 \frac{x}{L} + b_2 \frac{x}{L} \Rightarrow b(x) = b_1 + \frac{x}{L}(b_2 - b_1) * \frac{b_1}{b_1}$$

$$\Rightarrow b(x) = b_1 \left(1 + (\frac{b_2 - b_1}{b_1}) * \frac{x}{L} \right) \tag{3.2}$$

$$(\frac{b_2 - b_1}{b_1}) = \alpha$$

Where α is the taper ratio for the varying cross-sectional beam.

The b(x) term for varying cross-sectional beam is obtained as in Equation 3.3 with dependent on x displacement and alfa taper ratio parameters.

$$b(x) = b_1 \left[1 + \alpha \frac{x}{L} \right] \tag{3.3}$$

The A(x) term is obtained as in Equation 3.4 with x dependent.

$$\begin{aligned} A(x) &= b(x) * h \\ &= b_1 \left(1 + \alpha \frac{x}{L} \right) * h \\ \Rightarrow A(x) &= A_1 \left[1 + \alpha \frac{x}{L} \right] \end{aligned} \tag{3.4}$$

The area moment of inertia for varying cross-sectional beam is found as given following,

$$I_{zz}(x) = b(x)\frac{h^3}{12}$$

$$= b_1\left[1+\alpha\frac{x}{L}\right]\frac{h^3}{12} \tag{3.5}$$

$$\Rightarrow I_{zz}(x) = I_{zz1}\left[1+\alpha\frac{x}{L}\right]$$

The strain energy for the varying cross-sectional beam is given by (Benosman & Cosmotsa, 1992)

$$U = \frac{1}{2}\int_0^L \frac{M(x)^2}{EI_{zz}(x)}dx \tag{3.6}$$

Where M(x) is bending moment, E is modulus of elasticity and I is area moment of inertia.

The bending moment at first node is given by;

$$M(x) = Q_1.x - M_1$$

$$M(x)^2 = {Q_1}^2.x^2 + {M_1}^2 - 2Q_1.M_1.x$$

$$v_1 = \frac{du}{dQ_1} \tag{3.7}$$

$$\theta_1 = \frac{du}{dM_1} \tag{3.8}$$

$$\frac{du}{dQ_1} = \int_0^L \frac{1}{2}\left(\frac{{Q_1}^2.x^2 - 2Q_1.x.M_1 + {M_1}^2}{EI_{zz}(x)}\right)dx \tag{3.9}$$

$$\frac{du}{dM_1} = \int_0^L \frac{1}{2}\left(\frac{{Q_1}^2.x^2 - 2Q_1.x.M_1 + {M_1}^2}{EI_{zz}(x)} \right) dx \tag{3.10}$$

The stiffness matrix for the first node of the finite element is obtained as below,

$$\begin{Bmatrix} v_1 \\ \theta_1 \end{Bmatrix} = \begin{bmatrix} \int_0^L \frac{x^2}{EI_{zz}(x)} dx & -\int_0^L \frac{x}{EI_{zz}(x)} dx \\ -\int_0^L \frac{x}{EI_{zz}(x)} dx & \int_0^L \frac{1}{EI_{zz}(x)} dx \end{bmatrix} \begin{Bmatrix} Q_1 \\ M_1 \end{Bmatrix}$$

$$A_i = \int_0^L \frac{x^{(i-1)}}{EI_{zz}(x)} dx, \qquad i = 1,\ 2 \ \ and \ \ 3. \tag{3.11}$$

$$\Rightarrow \begin{Bmatrix} v_1 \\ \theta_1 \end{Bmatrix} = \begin{bmatrix} A_3 & -A_2 \\ -A_2 & A_1 \end{bmatrix}$$

The bending moment at 2.node is given by;

$$M(x) = -Q_2.(L - .x) + M_2$$

$$M(x)^2 = {Q_2}^2.L^2 + {Q_2}^2.x^2 + 2Q_2.L.x + {M_2}^2 - 2Q_2.M_2.(L - x)$$

$$v_2 = \frac{du}{dQ_2} \tag{3.12}$$

$$\theta_2 = \frac{du}{dM_2} \tag{3.13}$$

$$U = \frac{1}{2}\int_0^L \frac{M(x)^2}{EI_{zz}(x)} dx = \frac{1}{2}\int_0^L \frac{\left({Q_2}^2.L^2 + {Q_2}^2.x^2 + 2Q_2.L.x + {M_2}^2 - 2Q_2.M_2.(L - x)\right)}{EI_{zz}(x)} dx$$

$$\frac{du}{dQ_2}=\int_0^L\frac{1}{2}\left(\frac{{Q_2}^2.L^2+{Q_2}^2.x^2+2Q_2.L.x+{M_2}^2-2Q_2.M_2.(L-x)}{EI_{zz}(x)}\right)dx$$

$$\frac{du}{dM_2}=\int_0^L\frac{1}{2}\left(\frac{{Q_2}^2.L^2+{Q_2}^2.x^2+2Q_2.L.x+{M_2}^2-2Q_2.M_2.(L-x)}{EI_{zz}(x)}\right)dx$$

The stiffness matrix for the second node of the finite element is obtained as below

$$\begin{Bmatrix}v_2\\ \theta_2\end{Bmatrix}=\begin{bmatrix}\int_0^L\frac{(L-x)^2}{EI_{zz}(x)}dx & \int_0^L\frac{(L-x)}{EI_{zz}(x)}dx\\ \int_0^L\frac{(L-x)}{EI_{zz}(x)}dx & \int_0^L\frac{1}{EI_{zz}(x)}dx\end{bmatrix}\begin{Bmatrix}Q_2\\ M_2\end{Bmatrix}$$

$$B_i=\int_0^L\frac{(L-x)^{(i-1)}}{EI_{zz}(x)}dx,\qquad i=1,\ 2\ \ and\ \ 3. \tag{3.14}$$

$$\Rightarrow\begin{Bmatrix}v_2\\ \theta_2\end{Bmatrix}=\begin{bmatrix}B_3 & B_2\\ B_2 & B_1\end{bmatrix}\begin{Bmatrix}Q_2\\ M_2\end{Bmatrix}\qquad at\ \ the\ \ 2.node$$

$$E.I_{zz}(x)=E.I_{zz1}\left[1+\alpha.\frac{x}{L}\right] \tag{3.15}$$

$$E.A(x)=E.A_1\left[1+\alpha.\frac{x}{L}\right] \tag{3.16}$$

$$A_i=\int\frac{x^{(i-1)}}{EI_{zz}(x)}dx,\qquad i=1,2,3 \tag{3.17}$$

$$D_1=A_1.A_3-A_2.A_2 \tag{3.18}$$

The obtaining element stiffness matrix for axial displacement is given below,

$$C = \int_0^L \frac{1}{A(x)E}\,dx = \frac{1}{EA_1}\int_0^L \frac{1}{(1+\alpha.\frac{x}{L})}.dx$$

$$\Rightarrow C = \frac{1}{EA_1}\frac{L}{\alpha}\left(\ln(\alpha+1)\right) \tag{3.19}$$

The following exact stiffness matrix can be found by combining the obtained axial and the transverse stiffness matrix for a general beam element,

$$K = \begin{bmatrix} k_{11}^{\ A} & k_{12}=0 & k_{13}=0 & k_{12}^{\ A} & k_{15}=0 & k_{16}=0 \\ k_{21}=0 & k_{11}^{\ B} & k_{12}^{\ B} & k_{24}=0 & k_{13}^{\ B} & k_{14}^{\ B} \\ k_{31}=0 & k_{21}^{\ B} & k_{22}^{\ B} & k_{34}=0 & k_{23}^{\ B} & k_{24}^{\ B} \\ k_{21}^{\ A} & k_{42}=0 & k_{43}=0 & k_{22}^{\ A} & k_{45}=0 & k_{46}=0 \\ k_{51}=0 & k_{31}^{\ B} & k_{32}^{\ B} & k_{54}=0 & k_{33}^{\ B} & k_{34}^{\ B} \\ k_{61}=0 & k_{41}^{\ B} & k_{42}^{\ B} & k_{64}=0 & k_{43}^{\ B} & k_{44}^{\ B} \end{bmatrix} \tag{3.20}$$

$$k_{11} = k_{44} = -k_{14} = -k_{41} = \frac{1}{C} = \frac{EA_1}{L}\left[\frac{\alpha}{\ln(\alpha+1)}\right] \tag{3.21}$$

$$k_{22} = k_{55} = -k_{15} = -k_{51} = \frac{A_1}{D_1} = \frac{EI_{zz1}}{L^3}\left[\frac{2\alpha^2.\ln(\alpha+1)}{(\alpha+2).\ln(\alpha+1)-2\alpha}\right] \tag{3.22}$$

$$k_{12} = k_{21} = 0, \qquad k_{13} = k_{31} = 0, \qquad k_{15} = k_{51} = 0, \qquad k_{16} = k_{61} = 0 \tag{3.23}$$

$$\frac{A_2}{D_1} = \frac{EI_{zz1}}{L^2}\left[\frac{2\alpha.(\alpha-\ln(\alpha+1))}{(\alpha+2).\ln(\alpha+1)-2\alpha}\right] \tag{3.25}$$

$$\frac{A_3}{D_1} = \frac{EI_{zz1}}{L}\left[\frac{2.\ln(\alpha+1)+\alpha(\alpha-2)}{(\alpha+2).\ln(\alpha+1)-2\alpha}\right] \tag{3.26}$$

The stiffness matrix in local coordinates can be obtained by combining the resulting axial and transverse stiffness matrix for a beam element. The obtained element exact stiffness matrix for a linearly tapered beam is shown below,

$$[K]=\begin{bmatrix} \frac{1}{C} & 0 & 0 & -\frac{1}{C} & 0 & 0 \\ 0 & \frac{A_1}{D_1} & \frac{A_2}{D_1} & 0 & -\frac{A_1}{D_1} & L\frac{A_1}{D_1}-\frac{A_2}{D_1} \\ 0 & \frac{A_2}{D_1} & \frac{A_3}{D_1} & 0 & -\frac{A_2}{D_1} & L\frac{A_2.}{D_1}-\frac{A_3}{D_1} \\ -\frac{1}{C} & 0 & 0 & \frac{1}{C} & 0 & 0 \\ 0 & -\frac{A_1}{D_1} & -\frac{A_2}{D_1} & 0 & \frac{A_1}{D_1} & \frac{A_2-A_1.L}{D_1} \\ 0 & \frac{A_1.L-A_2}{D_1} & \frac{A_2.L-A_3}{D_1} & 0 & \frac{A_2-A_1.L}{D_1} & \frac{A_1L^2-2A_2.L+A_3}{D_1} \end{bmatrix} \quad (3.27)$$

3.3 Obtaining the Element Mass Matrix for a Varying Cross-section

The mass matrix in local coordinates can be obtained by combining the resulting axial and transverse mass matrix by the same procedures. The obtained mass matrix for a finite element beam is shown below,

$$[m]^A=\rho\int_0^L\begin{bmatrix}\frac{L-x}{L} & \frac{x}{L}\end{bmatrix}\begin{bmatrix}\frac{L-x}{L} \\ \frac{x}{L}\end{bmatrix}.A(x).dx \quad (3.28)$$

$$m_{11}{}^A=\frac{1}{12}\rho.A_1L(\alpha+4) \quad (3.29)$$

$$m_{12}{}^{A} = \frac{1}{12}\rho.A_1 L(\alpha + 2) \tag{3.30}$$

$$m_{21}{}^{A} = \frac{1}{12}\rho.A_1 L(\alpha + 2) \tag{3.31}$$

$$m_{12}{}^{A} = \frac{1}{12}\rho.A_1 L(3.\alpha + 2) \tag{3.32}$$

The shape functions for the bending displacements are given by

$$[m]^{A} = \rho\int_0^L \begin{bmatrix} \frac{L-x}{L} & \frac{x}{L} \end{bmatrix} \begin{bmatrix} \frac{L-x}{L} \\ \\ \frac{x}{L} \end{bmatrix} .A(x).dx \tag{3.33}$$

$$v(x) = H_1(x)v_1 + H_2(x)\theta_1 + H_3(x)v_2 + H_4(x)\theta_2 \tag{3.34}$$

Where,

$$[m]^{B} = \int_0^L \rho[H][H]^{T} A(x).dx \tag{3.35}$$

$$[H] = [H_1 \quad H_2 \quad H_3 \quad H_4] \tag{3.36}$$

$$[m]^{B} = \rho\int_0^L \begin{bmatrix} 1-\frac{3x^2}{L^2}+\frac{2x^3}{L^3} & x-\frac{2x^2}{L}+\frac{x^3}{L^2} & \frac{3x^2}{L^2}-\frac{2x^3}{L^3} & -\frac{x^2}{L}+\frac{x^3}{L^2} \end{bmatrix} \begin{bmatrix} 1-\frac{3x^2}{L^2}+\frac{2x^3}{L^3} \\ x-\frac{2x^2}{L}+\frac{x^3}{L^2} \\ \frac{3x^2}{L^2}-\frac{2x^3}{L^3} \\ -\frac{x^2}{L}+\frac{x^3}{L^2} \end{bmatrix} .A(x).dx$$

$$H_1(x) = 1 - \frac{3x^2}{L^2} + \frac{2x^3}{L^3}$$

$$H_2(x) = x - \frac{2x^2}{L} + \frac{x^3}{L^2}$$

$$H_3(x) = \frac{3x^2}{L^2} - \frac{2x^3}{L^3} \tag{3.37}$$

$$H_4(x) = -\frac{x^2}{L} + \frac{x^3}{L^2}$$

The obtained exact element mass matrix of the tapered beam is shown below,

$$[M] = \begin{bmatrix} m_{11}^{\ A} & m_{12}=0 & m_{13}=0 & m_{12}^{\ A} & m_{15}=0 & m_{16}=0 \\ m_{21}=0 & m_{11}^{\ B} & m_{12}^{\ B} & m_{24}=0 & m_{13}^{\ B} & m_{14}^{\ B} \\ m_{31}=0 & m_{21}^{\ B} & m_{22}^{\ B} & m_{34}=0 & m_{23}^{\ B} & m_{24}^{\ B} \\ m_{21}^{\ A} & m_{42}=0 & m_{43}=0 & m_{22}^{\ A} & m_{45}=0 & m_{46}=0 \\ m_{51}=0 & m_{31}^{\ B} & m_{32}^{\ B} & m_{54}=0 & m_{33}^{\ B} & m_{34}^{\ B} \\ m_{61}=0 & m_{41}^{\ B} & m_{42}^{\ B} & m_{64}=0 & m_{43}^{\ B} & m_{44}^{\ B} \end{bmatrix} \tag{3.38}$$

$$m_{11}^{\ B} = \frac{1}{35}\rho.A_1 L(3.\alpha + 13) \tag{3.39}$$

$$m_{12}^{\ B} = \frac{1}{420}\rho.A_1 L^2(7.\alpha + 22) \tag{3.40}$$

$$m_{13}^{\ B} = \frac{1}{140}\rho.A_1 L(\alpha + 2) \tag{3.41}$$

$$m_{14}^{\ B} = \frac{1}{420}\rho.A_1 L^2(6.\alpha + 13) \tag{3.42}$$

$$m_{22}{}^{B} = \frac{1}{840}\rho.A_1L^3(3.\alpha+8) \tag{3.43}$$

$$m_{23}{}^{B} = \frac{1}{420}\rho.A_1L^2(7.\alpha+13) \tag{3.44}$$

$$m_{24}{}^{B} = -\frac{1}{280}\rho.A_1L^3(\alpha+2) \tag{3.45}$$

$$m_{33}{}^{B} = \frac{1}{35}\rho.A_1L(10.\alpha+13) \tag{3.46}$$

$$m_{34}{}^{B} = -\frac{1}{420}\rho.A_1L^2(15.\alpha+22) \tag{3.47}$$

$$m_{44}{}^{B} = \frac{1}{840}\rho.A_1L^3(5.\alpha+8) \tag{3.48}$$

3.4 The Distributed Inertia Forces

The distributed inertia forces for the varying cross-section and rectangular beam are given in Figure 3.4. Where q_{nx}, and q_{ny} is the distributed forces for FE-n. The forces can be written as follows;

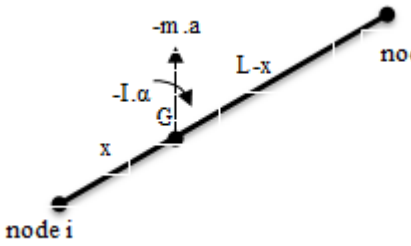

$$q_{ny} = -\rho.V.a_{Gy}$$

$$q_{nx} = -\rho.V.a_{Gx}$$

Figure 3.4 The distributed forces for a finite element

For example, the nodal forces for Node-6 are formed due to the distributed forces for FE-3 and FE-4. So, the following can be written for the elements of the nodal force vector, $\mathbf{f}_s$, corresponding to Node-6.

$$f_s(9,1) = q_{3x}.\frac{x_{G3}}{h_3} + q_{4x}.\frac{h_4 - x_{G4}}{h_4}$$

$$f_s(10,1) = q_{3y}.\frac{x_{G3}}{h_3} + q_{4y}.\frac{h_4 - x_{G4}}{h_4}$$

CHAPTER FOUR
EXPERIMENTAL VIBRATION ANALYSIS OF TWO-LINK MANIPULATORS

4.1 Introduction

There are three experimental systems considered. The second studied manipulator system is similar to the first considered manipulator system. The first manipulator has varying cross-section and the second manipulator has uniform cross-section. The weight, length, thickness and material properties are same for the two similar manipulator systems.

4.2 Experimental Systems

The studied experimental systems were labeled sy1_varying_al2, sy2_eq_uniform_al2 and sy3_varying_al2.

4.2.1 Two-link Manipulator 1 (sy1_varying_al2)

The two-link tapered flexible manipulator system is shown in figure 4.1. The links have varying cross-section. The link material is aluminum alloy.

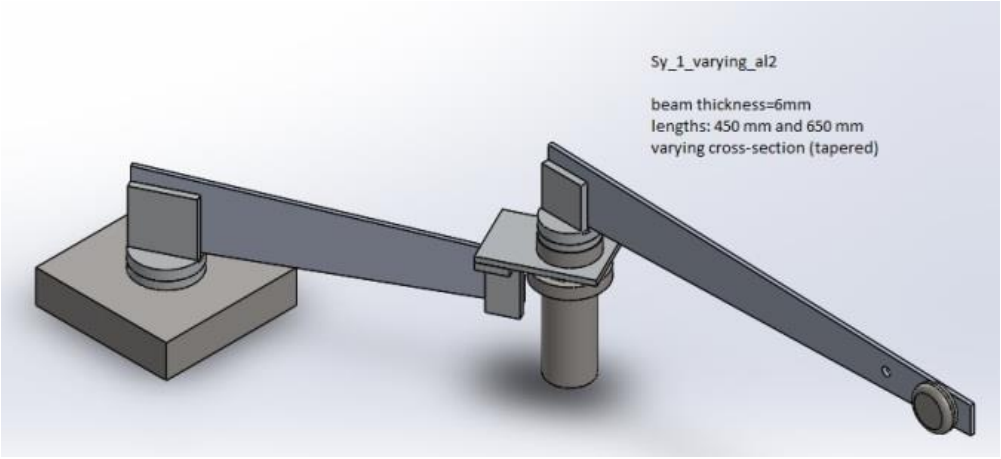

Figure 4.1 The Solidworks model of the Sy1_varying_al2

Figure 4.2 The experimental prototype of the Sy1_varying (Personal archive, 2017)

Table 4.1 Physical properties of the two-link flexible manipulator (sy1_varying_al2)

Property	Flexible Arm 1	Flexible Arm 2
Material	Aluminum	Aluminum
Density	2700 kg/m^3	2700 kg/m^3
Modulus of Elasticity (GPa)	71GPa	71GPa
Poisson's Ratio	0.33	0.33
Material Damping	α=0, β=0.00038	α=0, β=0.00038
Length (mm)	450	650
Height-1 of the cross-section (mm)	100	80
Height-2 of the cross-section (mm)	60	40
Width of the cross-section (mm)	6	6
Flexible joint torsional stiffness	16000Nm/r	16000Nm/r
Finite element number	ne2=20	ne3=40

4.2.2 Two-link Manipulator 2 (sy2_eq_uniform_al2)

The two-link flexible manipulator system is shown in below figure. The system is approximately equivalent to Sy1_varying_al2 system. The links have uniform cross-section. The link material is aluminum alloy.

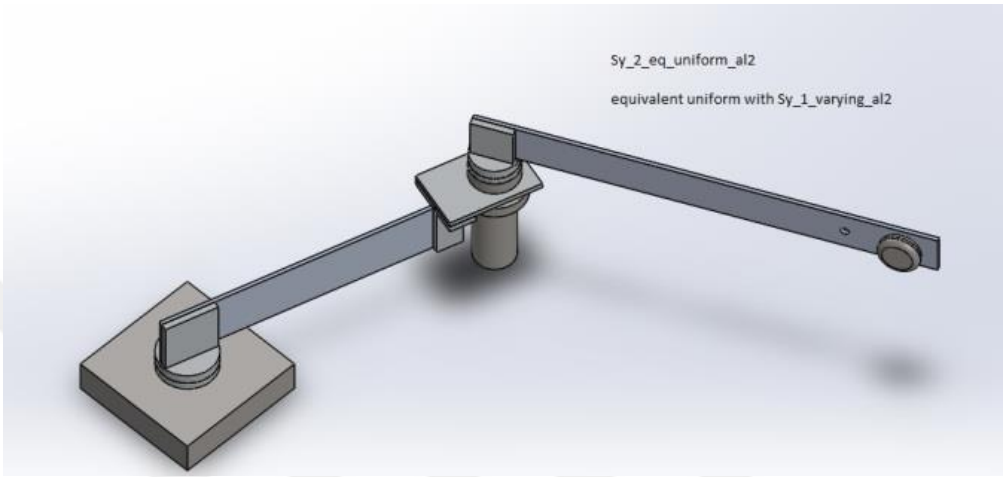

Figure 4.3 The solidworks model of the Sy2_eq_uniform_al2

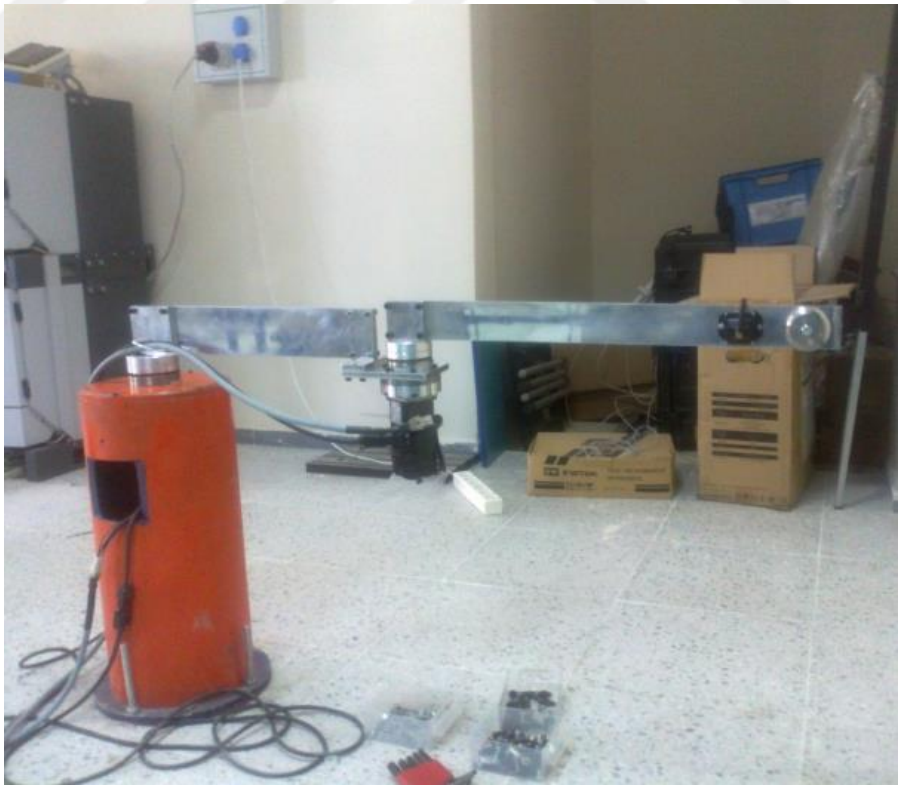

Figure 4.4 The experimental prototype of the Sy2_eq_uniform_al2 (Personel archive, 2017)

Table 4.2 Physical properties of the two-link flexible manipulator (sy2_eq_uniform)

Property	Flexible Arm 1	Flexible Arm 2
Material	Aluminum	Aluminum
Density	2700 kg/m^3	2700 kg/m^3
Modulus of Elasticity (GPa)	71Gpa	71GPa
Poisson's Ratio	0.33	0.33
Material Damping	α=0 and	α=0 and
Length (mm)	450	650
Height of the cross-section (mm)	80	60
Width of the cross-section (mm)	6	6
Flexible joint torsional stiffness	16000Nm/r	16000Nm/r
Finite element number	ne2=20	ne3=40

4.2.3 Two-link Manipulator 3 (sy3_varying_al2)

The two-link tapered flexible manipulator system is shown in figure below. The links have varying cross-section. The link material is aluminum alloy. The link thickness is 5 mm. The length1 and length2 is 500mm and 700mm, respectively. The model has not payload because the system is very flexible.

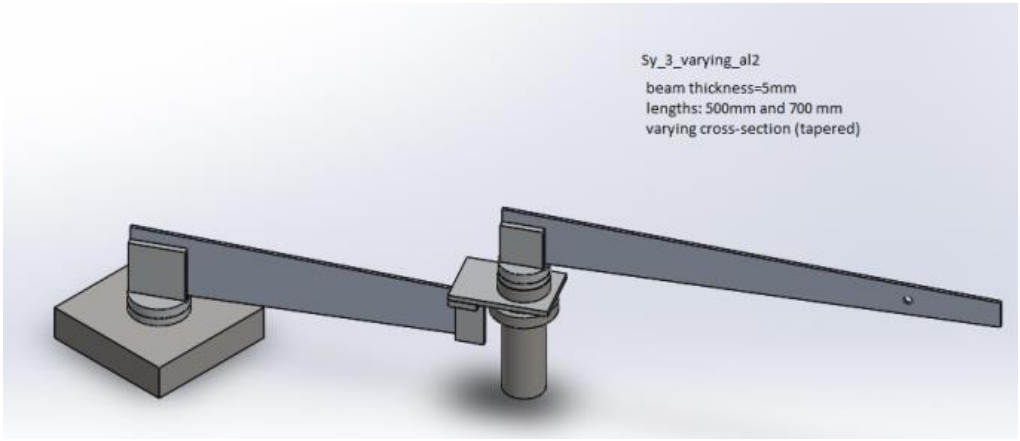

Figure 4.5 The solidworks model of the Sy3_varying_al2

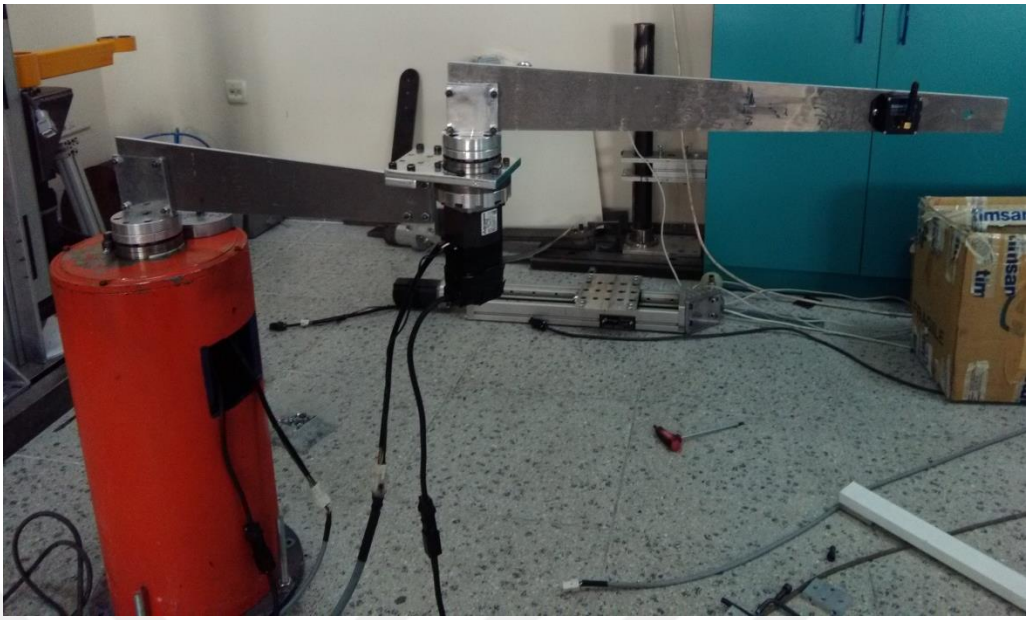

Figure 4.6 The experimental prototype of the Sy3_varying_al2 (Personal archive, 2017)

Table 4.3 The physical properties of Sy3_varying_al2

Property	Flexible Arm 1	Flexible Arm 2
Material	Aluminum	Aluminum
Density	2700 kg/m^3	2700 kg/m^3
Modulus of Elasticity (GPa)	71GPa	71GPa
Poisson's Ratio	0.33	0.33
Material Damping	α=0 and	α=0 and
Length (mm)	500	700
Height-1 of the cross-section (mm)	100	80
Height-2 of the cross-section (mm)	70	40
Width of the cross-section (mm)	5	5
Flexible joint torsional stiffness	16000Nm/r	16000Nm/r
Finite element number	ne2=20	ne3=40

4.3 The Measurement System

The manipulator is produced for the experiments. The experimental set-up consists of two-link flexible tapered manipulator, two Mitsubishi servo motors and drivers, a motion control card, a wireless accelerometer sensor, a wireless data acquisition system (WDA) and a PC. The wireless sensor is located at the end of the manipulators in the experiments.

Two different accelerationmeter sensor and measurement system are used. The considered measurement system is shown in Figure 4.7. The wireless vibration sensor is a MicroStrain G-Link tri-axial accelerometer (Accelerometer range: ± 10g, 47 g, 58 mm x 43 mm x 26 mm). The wireless base station is MicroStrain Gateway WSDA-Base-104.

Figure 4.7 The used wireless accelerationmeter sensor (Personal archive, 2016)

Mitsubishi Electric servo motors and drivers with 200 W, Model HC-KFS23B/ MR-J2S-20A, are used. Harmonic Drive gearboxs with the gear ratio of 80 and 100 is used for the servo motors. A PC-based motion control card, Adlink PCI-8366 is used. The motion control card and driver are connected in serial by SSCNET network.

CHAPTER FIVE
RESIDUAL VIBRATION CONTROL OF TWO-LINK MANIPULATORS WITH LINEARLY TAPERED BEAMS

5.1 Introduction

In the section, the vibration signals, modal analysis results, transient analysis results and graphics were obtained from developed Matlab codes based on finite element theory and Newmark numerical integration.

5.2 Modal Analysis Results

Three end-point positions of the system are considered, and they are listed in following Table.

Table 5.1 Modal analysis results for the analyzed case positions

Location	ϕ_{2s}	ϕ_{3s}	**Sy1_varying_al2 First natural frequency f1 (Hz)**			**Sy2_eq_uniform_al2**		**Sy3_varying_al2 (without payload)**	
			Sim-1-M1	**Sim-1-M2**	**Exp-1**	**Sim-2**	**Exp-2**	**Sim-3-M2**	**Exp-3**
F Flexible	0^o	0^o	2.8461	2.8706	2.9374	2.70	2.71	2.5849	2.5608
S	45^o	90^o	3.3725	3.4033	3.6152	3.21	3.31	2.8423	2.7867
R Rigid	90^o	170^o	4.3461	4.3909	4.7450	4.17	4.22	3.1754	3.2386
Sim_M1: Matlab simulation with model-1 (direct formulation) Sim_M2: Matlab simulation with model-2 (varying function) Exp: Experimental accelerometer vibration signals									

5.2.1 Modal Analysis Results of Sy1_varying_al2

The modal analyses are performed for F, S and R locations of the two-link manipulator with tapered beams. The simulation results are obtained by the developed analysis program with MatLAB codes.

Table 5.1 Modal analysis results for the analyzed case positions

Location	ϕ_{2s}	ϕ_{3s}	Sy1_varying_al2 First natural frequency f1 (Hz)		
			Sim1_M1	Sim1_M2	Exp-1
F Flexible	0^o	0^o	2.8461	2.8706	2.9374
S Semi-Flexible	45^o	90^o	3.3725	3.4033	3.6152
R Rigid	90^o	170^o	4.3461	4.3909	4.7450

Where Sim1-M1 is MatLAB simulation with the model I, Sim1-M2 is MatLAB simulation with the model II, Exp-1 is experimental results for the Sy1-varyig-al2 system.

5.2.2 Modal Analysis Results of Sy2_uniform_al2

The modal analyses are performed for F, S and R locations of the two-link manipulator with uniform beams. The simulation results are obtained by the developed analysis program with MatLAB codes.

Table 5.2 Modal analysis results for the sy2-uniform-al2

Location	ϕ_{2s}	ϕ_{3s}	Sy2_eq_uniform_al2	
			Sim2	Exp-2
F - Flexible	0^o	0^o	2.70	2.71
S - Semi-Flexible	45^o	90^o	3.21	3.31
R - Rigid	90^o	170^o	4.17	4.22

5.2.3 Modal Analysis Results of Sy3_varying_al2

The modal analyses are performed for F, S and R locations of the two-link manipulator with uniform beams. The simulation results are obtained by the developed analysis program with MatLAB codes.

Table 5.3 Modal analysis results for the sy3-varying-al2

Location	ϕ_{2s}	ϕ_{3s}	**Sy3_varying_al2**	
			Sim3_M2 f_1 (Hz)	Exp-3
F- Flexible	0^o	0^o	2.5849	2.5608
S - Semi-Flexible	45^o	90^o	2.8423	2.7867
R - Rigid	90^o	170^o	3.1754 * 2.9346	3.2386 *3.0880
*: with tip mass (400gr)				

5.2.4 Comparing The Results

Table 5.4 Modal analysis results for the analyzed case positions

Location	ϕ_{2s}	ϕ_{3s}	**Sy1_varying_al2 First natural frequency f1 (Hz)**			**Sy2_eq_uniform_al2**	
			Sim1_M1	**Sim1_M2**	**Exp-1**	**Sim2**	**Exp-2**
F Flexible	0^o	0^o	2.8461	2.8706	2.9374	2.70	2.71
S Semi-Flexible	45^o	90^o	3.3725	3.4033	3.6152	3.21	3.31
R Rigid	90^o	170^o	4.3461	4.3909	4.7450	4.17	4.22

Where Sim1-M1 is Matlab simulation with the model I, Sim1-M2 is Matlab simulation with the model II.

Table 5.5 The considered manipulator positions for case studies

	The top view
q=[0,0] flexible (F) The flexible position	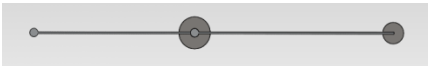
q=[45,90] semi-flexible (S) The semi-flexible position	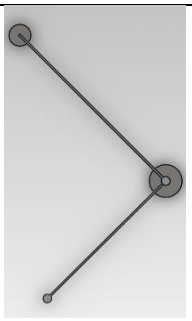
q=[90,170] rigid (R) The rigid position	

5.3 Case Studies for Residual Vibration Control

In the section, Case-FF, Case-FS, Case-FR and Case-SR were studied as experimental and numerical. In the analyses, while t_m was 2 and 3 seconds, t_{res} was 5 seconds.

Table 5.6 Setting of deceleration time for the target locations

Target Location	Case Study	$\mathbf{T_{decel}=k*T_1h}$ k=1,2,3,4	Sy1_varying_al2 First natural frequency f1 (Hz)			Sy2_eq_uniform_al2		Sy3_varying_al2 (without payload)	
			Sim-1-M1	**Sim-1-M2**	**Exp-1**	**Sim-2**	**Exp-2**	**Sim-3-M2**	**Exp-3**
F	Case-FF	$\mathbf{T_1h=(1/f_1)/2}$	2.8461	2.8706	2.934	2.70	2.71	2.5849	2.560
S	Case-FS	$\mathbf{T_1h=(1/f_1)/2}$	3.3725	3.4033	3.615	3.21	3.31	2.8423	2.786
R	Case-FR Case-SR	$\mathbf{T_1h=(1/f_1)/2}$	4.3461	4.3909	4.7450	4.17	4.22	3.1754	3.238

5.4 System Sy1_varying_al2

The considered system is shown in Figure 5.1. The manipulator links have linearly tapered beams.

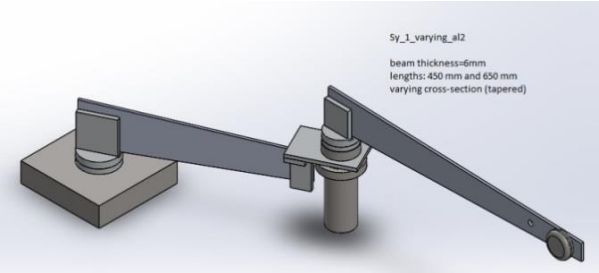

Figure 5.1 The sy1-varying-al2

5.4.1 Case FF Results

The starting position is Pos-f and the stopping position is Pos-f for Case-FF. The case properties are shown in Table 5.3.

Table 5.6 Case FF properties

Case	[t_{acc}, t_{con}, t_{dec}, t_m]	Starting pos.	Stopping pos.	Motor1	Motor2
Case-FF (1-2-3-4)	[*,T_{1h},T_{1h},3]	0-0	90-0	90	0
	[*,T_{1h},$2T_{1h}$,3]	0-0	90-0	90	0
	[*,T_{1h},$3T_{1h}$,3]	0-0	90-0	90	0
	[*,T_{1h},$4T_{1h}$,3]	0-0	90-0	90	0

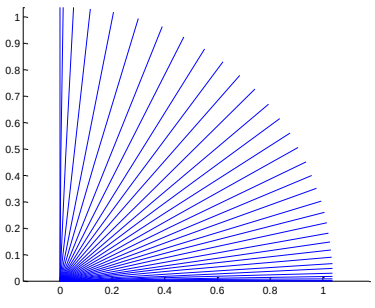

Case FF (90-0 from 0-0)

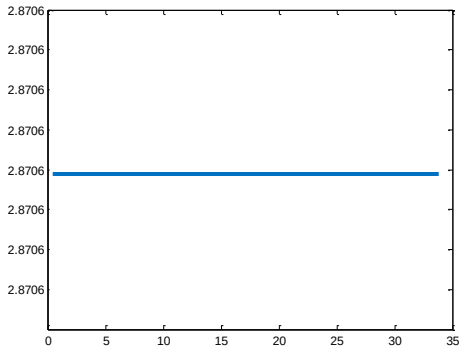

1.natural frequency for Case FF

Figure 5.1 The workspace for Case FF (f1=2.8706 Hz)

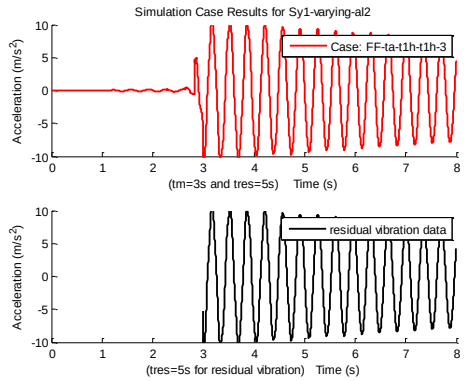	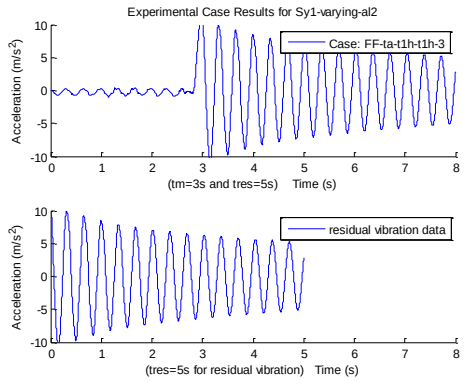
Matlab simulation Sim1-M2 RMS=6.5146	Experiment. RMS for the residual is 5.1251

Figure 5.2 CASE FF-1 (tm=3s, tres=5s)

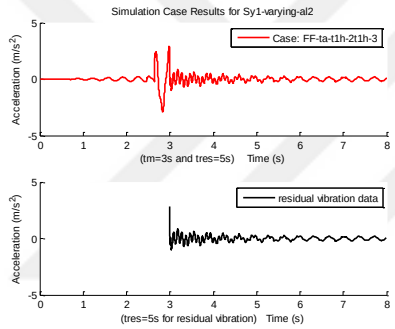	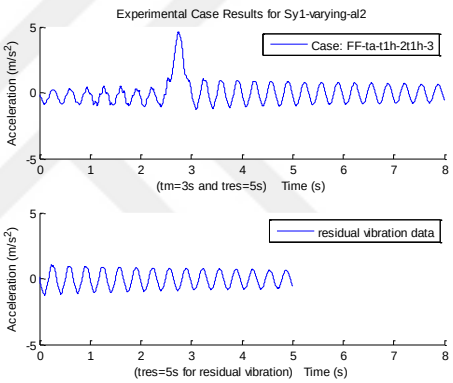
Matlab simulation Sim1-M2 RMS=0.2367	Experiment. RMS for the residual is 0.6246

Figure 5.3 CASE FF-2 (tm=3s, tres=5s)

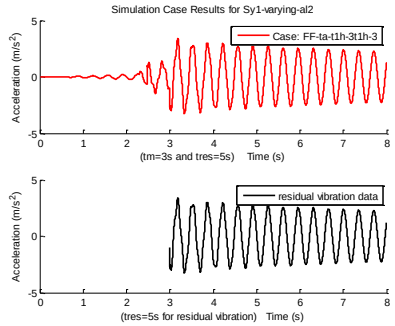

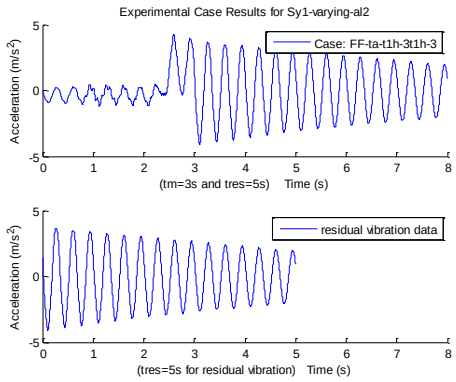

Matlab simulation Sim1-M2. RMS=1.8763	Experiment. RMS for the residual is 2.0778

Figure 5.4 CASE FF-3 (tm=3s, tres=5s)

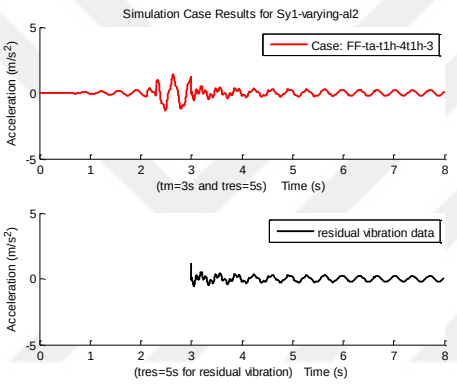

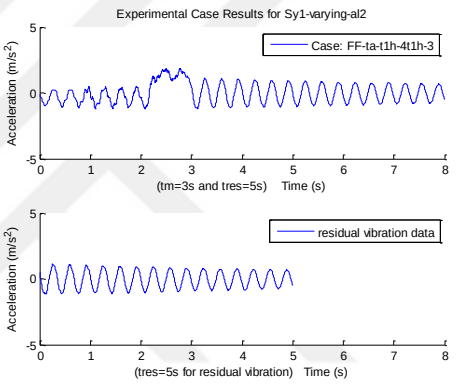

Matlab simulation Sim1-M2 RMS= 0.1925	Experiment.RMS for the residual is 0.6587

Figure 5.5 CASE FF-4 (tm=3s, tres=5s)

5.4.2 Case FS Results

The starting position is Pos-f and the stopping position is Pos-s for Case-FF. The Case properties are shown in Table 5.7.

Table 5.7 Case FS properties

Case	[t_{acc}, $t_{con,}t_{dec}$, t_m]	Starting pos.	Stopping pos.	Motor1	Motor2
Case-fs (1-2-3-4)	[*,T_{1h},T_{1h},3]	0-0	45 – 90 deg.	45 deg.	90 deg.
	[*,T_{1h},$2T_{1h}$,3]	0-0	45 – 90 deg.	45 deg.	90 deg.
	[*,T_{1h},$3T_{1h}$,3]	0-0	45 – 90 deg.	45 deg.	90 deg.
	[*,T_{1h},$4T_{1h}$,3]	0-0	45 – 90 deg.	45 deg.	90 deg.

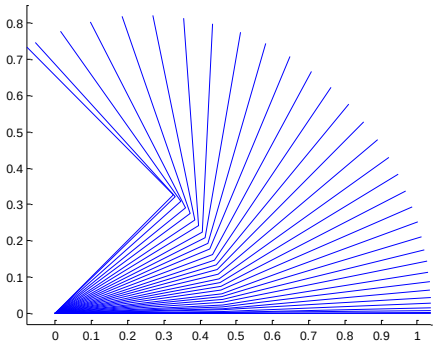	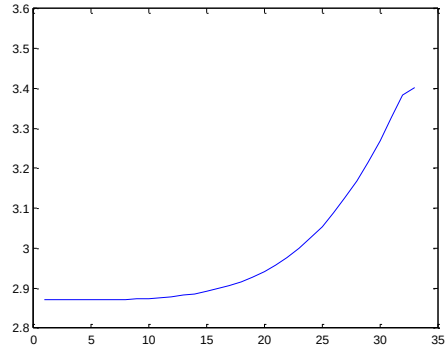
Case FF (90-0 from 0-0)	The change of 1.natural frequency for Case FS

Figure 5.6 The workspace for Case FS (f1=3.4033 Hz)

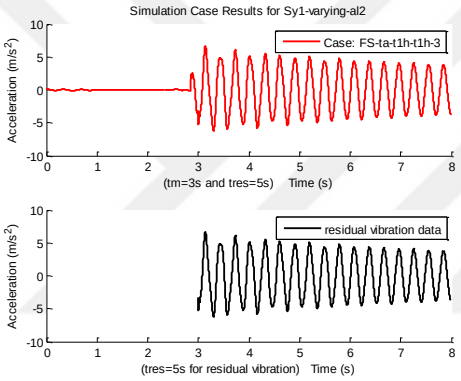	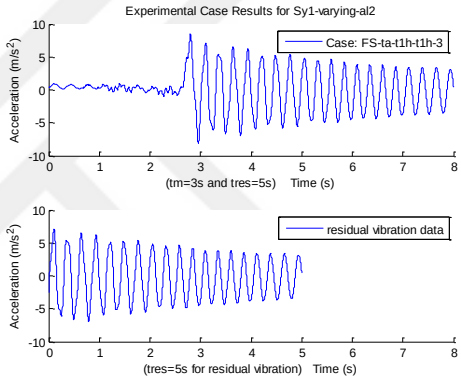
Matlab simulation Sim1-M2 .RMS =3.3927	Experiment. RMS for the residual is 3.4617

Figure 5.7 CASE FS-1 (tm=3s, tres=5s)

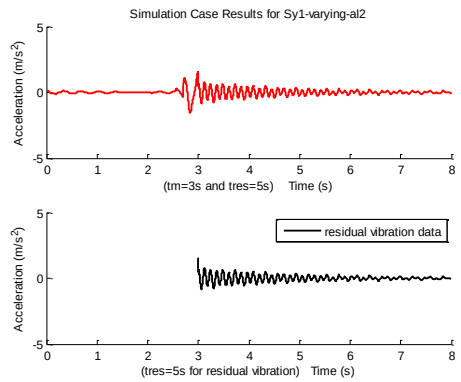	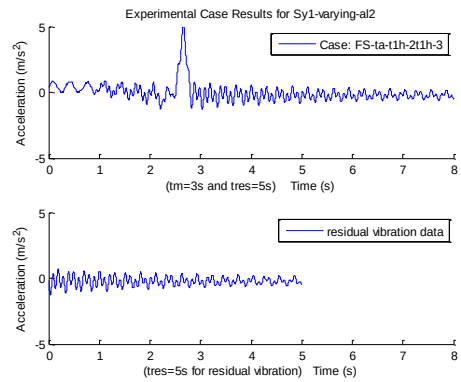
Matlab simulation Sim1-M2. RMS for the residual is 0.2432	Experiment RMS for the residual is 0.3993

Figure 5.8 CASE FS-2 (tm=3s, tres=5s)

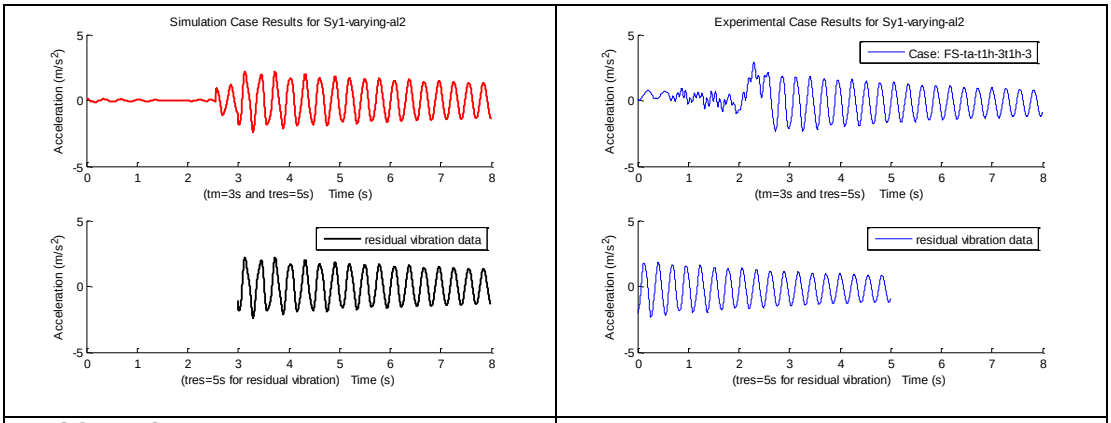

Matlab simulation Sim1-M2 RMS for the residual is 1.2055	Experiment RMS for the residual is 1.0640

Figure 5.9 CASE FS-3 (tm=3s, tres=5s)

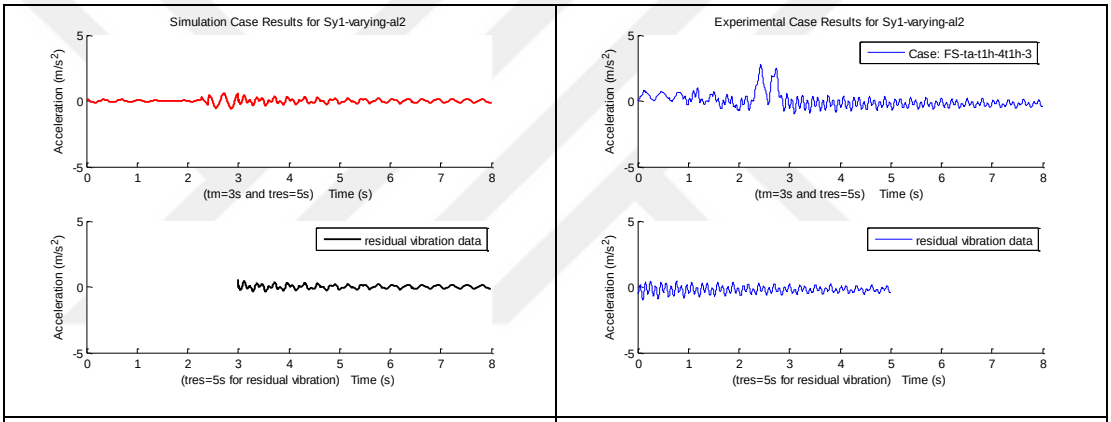

Matlab simulation RMS is 0.1371	Experiment RMS for the residual is 0.3408

Figure 5.10 CASE FS-4 (tm=3s, tres=5s)

5.4.3 Case FR Results

The starting position is Pos-f and the stopping position is Pos-r for Case-fr. The case properties are shown in Table 5.8.

Table 5.8 Case FS properties

Case	[t_{acc}, t_{con},t_{dec}, t_m]	Starting pos.	Stopping pos.	Motor1	Motor2
Case-fs (1-2-3-4)	[*,T_{1h},T_{1h},3]	0-0	90 – 170 deg.	90 deg.	170 deg.
	[*,T_{1h},$2T_{1h}$,3]	0-0	90 – 170 deg.	90 deg.	170 deg.
	[*,T_{1h},$3T_{1h}$,3]	0-0	90 – 170 deg.	90 deg.	170 deg.
	[*,T_{1h},$4T_{1h}$,3]	0-0	90 – 170 deg.	90 deg.	170 deg.

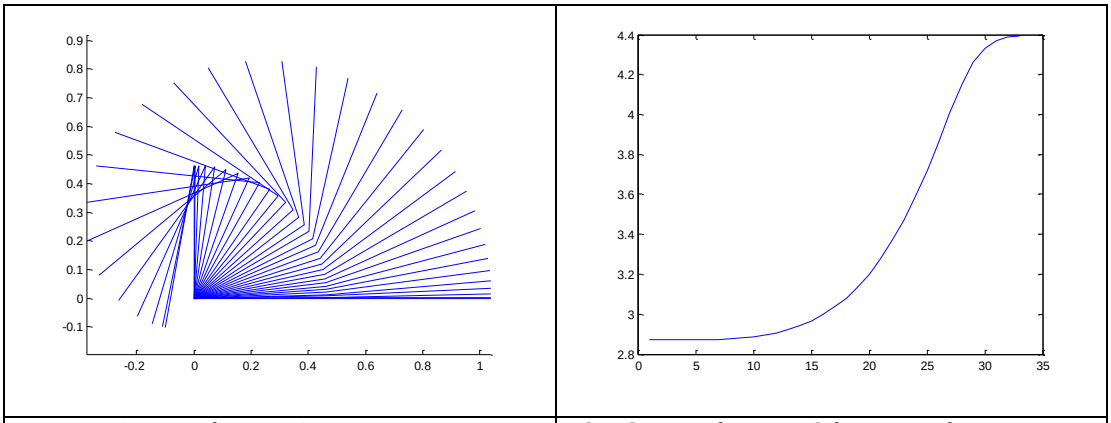

Case FR (90-170 from 0-0)	The change of 1.natural frequency for Case FR

Figure 5.11 The workspace for Case FR (f1= 4.3909 Hz)

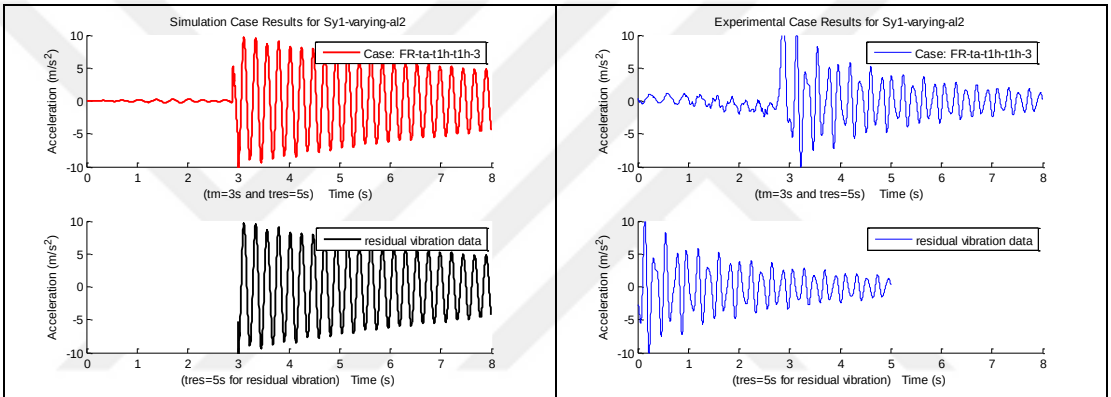

Matlab simulation Sim1-M2 RMS for the residual is 4.9797	Experiment RMS for the residual is 2.9151

Figure 5.12 CASE FR-1 (tm=3s, tres=5s)

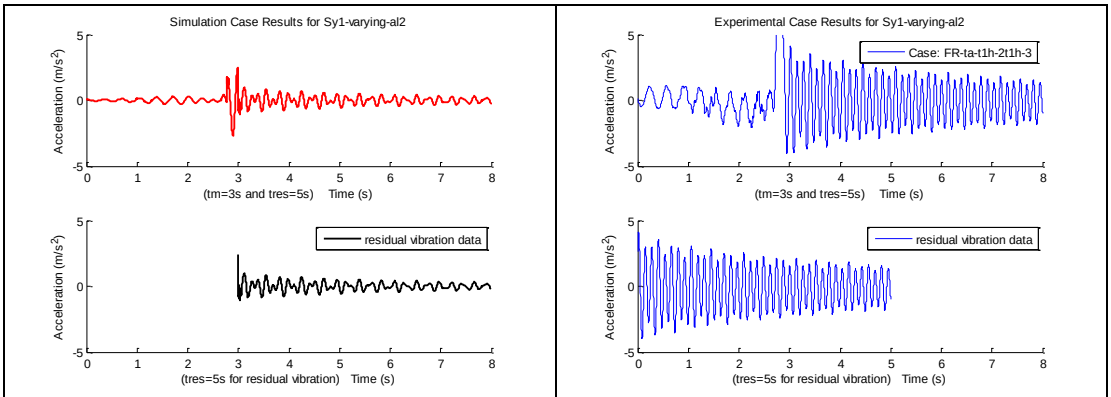

Matlab simulation Sim1-M2 RMS for the residual is 0.3245	Experiment RMS for the residual is 1.6551

Figure 5.13 CASE FR-2 (tm=3s, tres=5s)

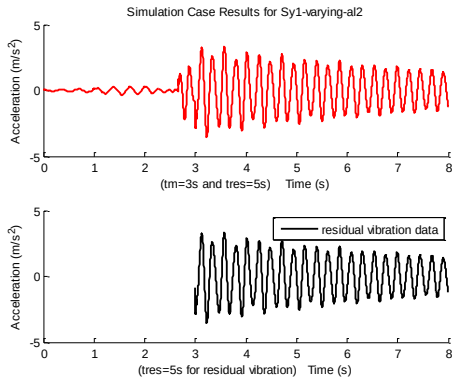

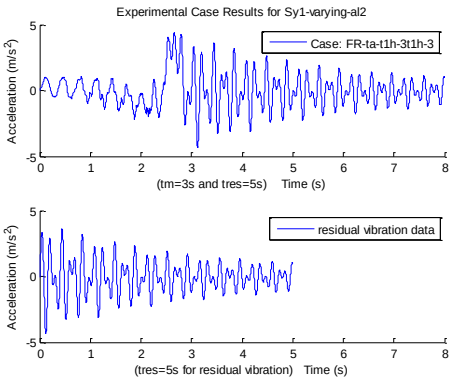

Matlab simulation Sim1-M2 RMS for the residual is 1.5886	Experiment RMS for the residual is 1.2543

Figure 5.14 CASE FR-3 (tm=3s, tres=5s)

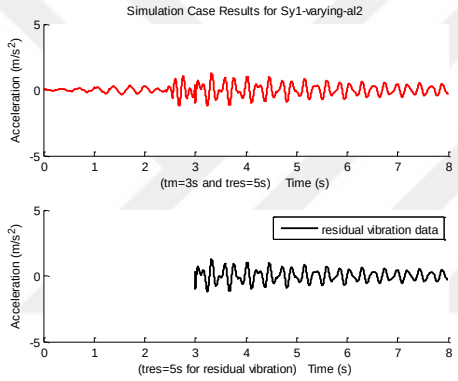

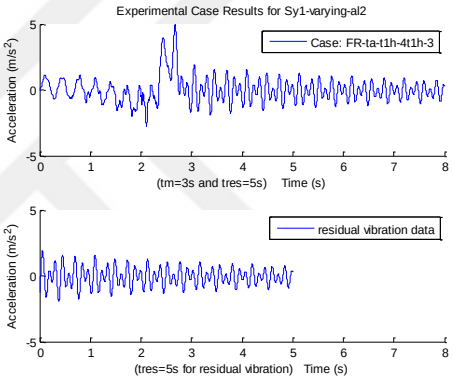

Matlab simulation RMS is 0.4527	Experiment RMS for the residual is 0.7084

Figure 5.15 CASE FR-4 (tm=3s, tres=5s)

5.4.4 Case SR Results

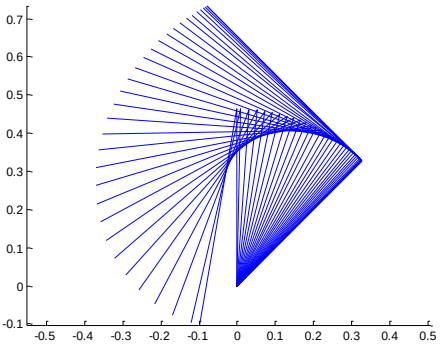

Case SR (90-170 from 0-90)

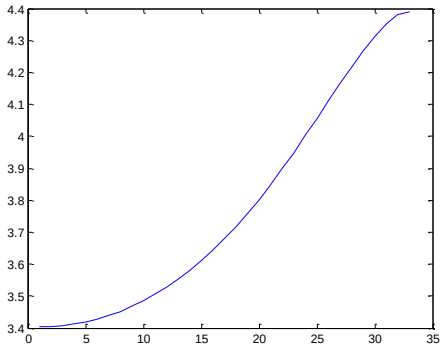

The change of 1.natural frequency for Case FR

The starting position is Pos-s and the stopping position is Pos-r for Case-sr. The case properties are shown in Table 5.9. The motion is from location S to location R.

Table 5.9 Case SR properties

Case	[t_{acc}, t_{con},t_{dec}, t_m]	Starting pos.	Stopping pos.	Motor1	Motor2
Case-SR (1-2-3-4)	[*,T_{1h},T_{1h},3]	45 – 90 deg.	90 – 170 deg.	45 deg.	80 deg.
	[*,T_{1h},$2T_{1h}$,3]	45 – 90 deg.	90 – 170 deg.	45 deg.	80 deg.
	[*,T_{1h},$3T_{1h}$,3]	45 – 90 deg.	90 – 170 deg.	45 deg.	80 deg.
	[*,T_{1h},$4T_{1h}$,3]	45 – 90 deg.	90 – 170 deg.	45 deg.	80 deg.

Figure 5.16 The workspace for Case FR (f1= 4.3909 Hz)

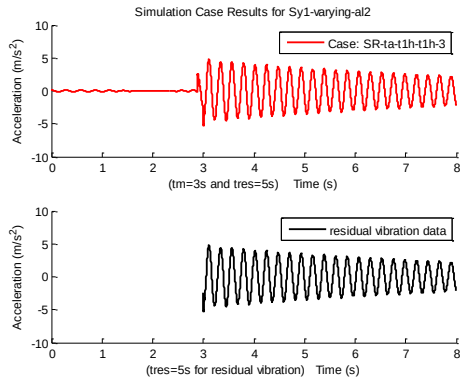

Matlab simulation Sim1-M2

RMS for the residual is 2.4056

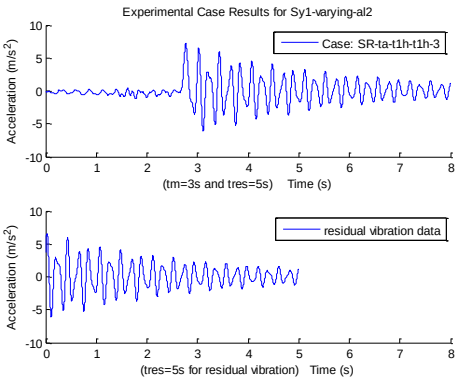

Experiment

RMS for the residual is 2.0137

Figure 5.17 CASE SR-1 (tm=3s, tres=5s)

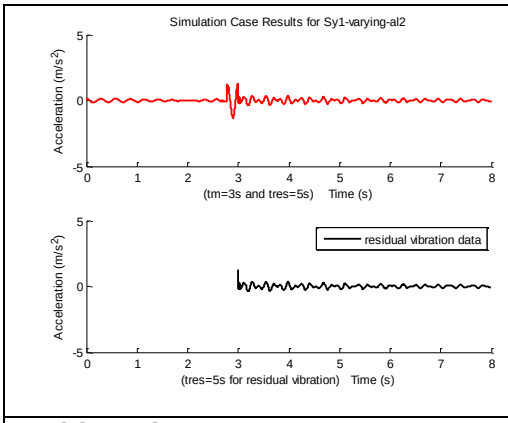	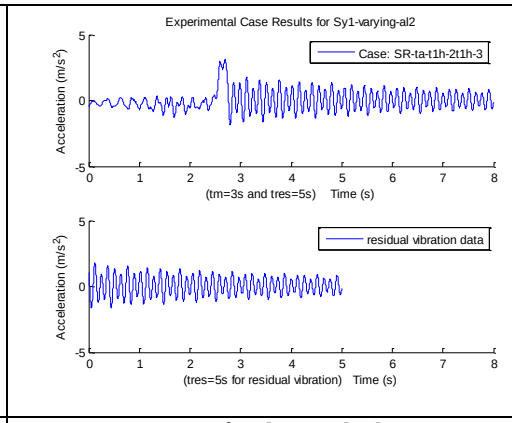
Matlab simulation Sim1-M2. RMS = 0.1326	Experiment. RMS for the residual is 0.7088

Figure 5.18 CASE SR-2 (tm=3s, tres=5s)

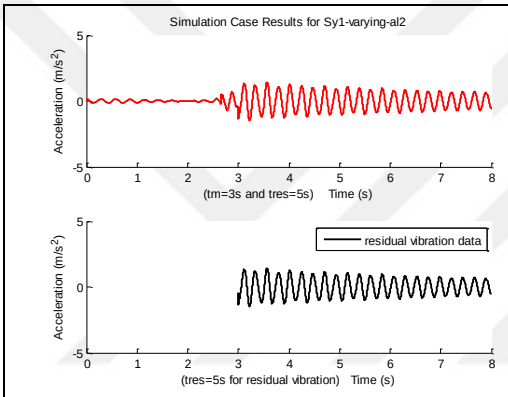	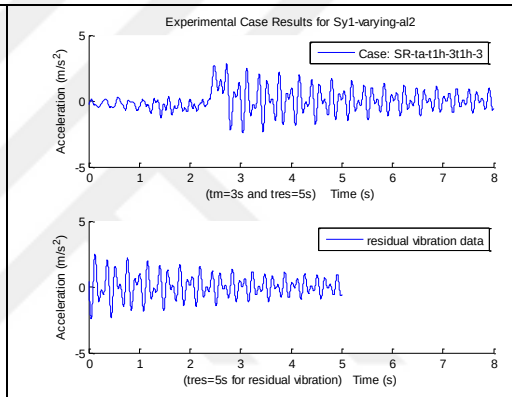
Matlab simulation Sim1-M2 RMS for the residual is 0.6988	Experiment RMS for the residual is 0.8410

Figure 5.19 CASE SR-3 (tm=3s, tres=5s)

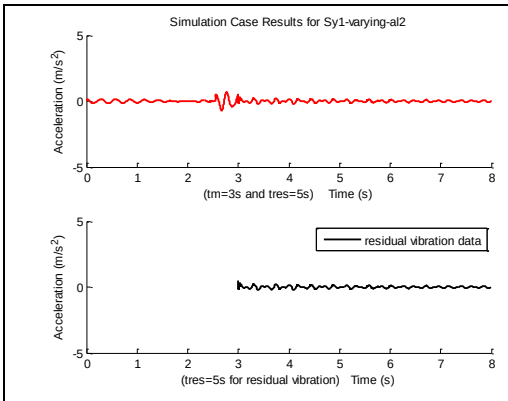	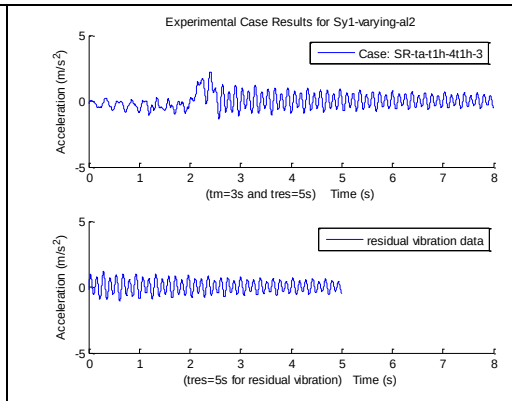
Matlab simulation Sim1-M2 rms is 0.0846	Experiment RMS for the residual is 0.4858

Figure 5.20 CASE SR-4 (tm=3s, tres=5s)

5.4.5 The rms results of the all cases for tm=3s

The comparison of the studied cases is shown in Table 5.10 for the sy1_varying_al2 and Sy2_eq_uniform_al2 two-link manipulator systems. It is observed that the residual vibration levels are high for td=t1h, and residual vibration levels are significantly decreased for td=2t1h.

Table 5.10 The rms results for all cases

Case	[t_{acc}, t_{con},t_{dec}, t_m]	Exp-2	Sim2	Sim1-M1	Sim1-M2	Exp-1
Case-FF	[*,T_{1h},T_{1h},3]	6.41	6.22	7.1425	6.5146	5.1251
	[*,T_{1h},$2T_{1h}$,3]	0.62	0.45	0.2728	0.2367	0.6246
	[*,T_{1h},$3T_{1h}$,3]	1.66	1.95	2.0106	1.8763	2.0778
	[*,T_{1h},$4T_{1h}$,3]	0.74	0.49	0.2055	0.1925	0.6587
Case-fs	[*,T_{1h},T_{1h},3]	3.49	3.56	4.5684	3.3927	3.4617
	[*,T_{1h},$2T_{1h}$,3]	0.31	0.19	0.2775	0.2432	0.3993
	[*,T_{1h},$3T_{1h}$,3]	1.27	1.04	1.5467	1.2055	1.0640
	[*,T_{1h},$4T_{1h}$,3]	0.31	0.19	0.2502	0.1371	0.3408
Case-fr	[*,T_{1h},T_{1h},3]	4.14	4.13	5.4369	4.9797	2.9151
	[*,T_{1h},$2T_{1h}$,3]	0.69	0.73	0.7818	0.3245	1.6551
	[*,T_{1h},$3T_{1h}$,3]	1.35	1.39	1.7468	1.5886	1.2543
	[*,T_{1h},$4T_{1h}$,3]	0.59	0.72	0.3443	0.4527	0.7084
Case-sr	[*,T_{1h},T_{1h},3]	2.49	1.99	2.8759	2.4056	2.0137
	[*,T_{1h},$2T_{1h}$,3]	0.35	0.29	0.3635	0.1326	0.7088
	[*,T_{1h},$3T_{1h}$,3]	0.69	0.65	0.9689	0.6988	0.8410
	[*,T_{1h},$4T_{1h}$,3]	0.34	0.16	0.1920	0.0846	0.4858

The comparing RMS plots for Case-FF and Case-fs is shown in Figure 5.21 and Figure 5.22, respectively. Analyzing the rms results of the motion inputs of the case, it is observed that the even multiples of the t1h parameter have more effective

reduction compared to odd multiples of t1h. It is observed that the residual vibration levels are high for td=t1h, and residual vibration levels are significantly decreased for td=2t1h.

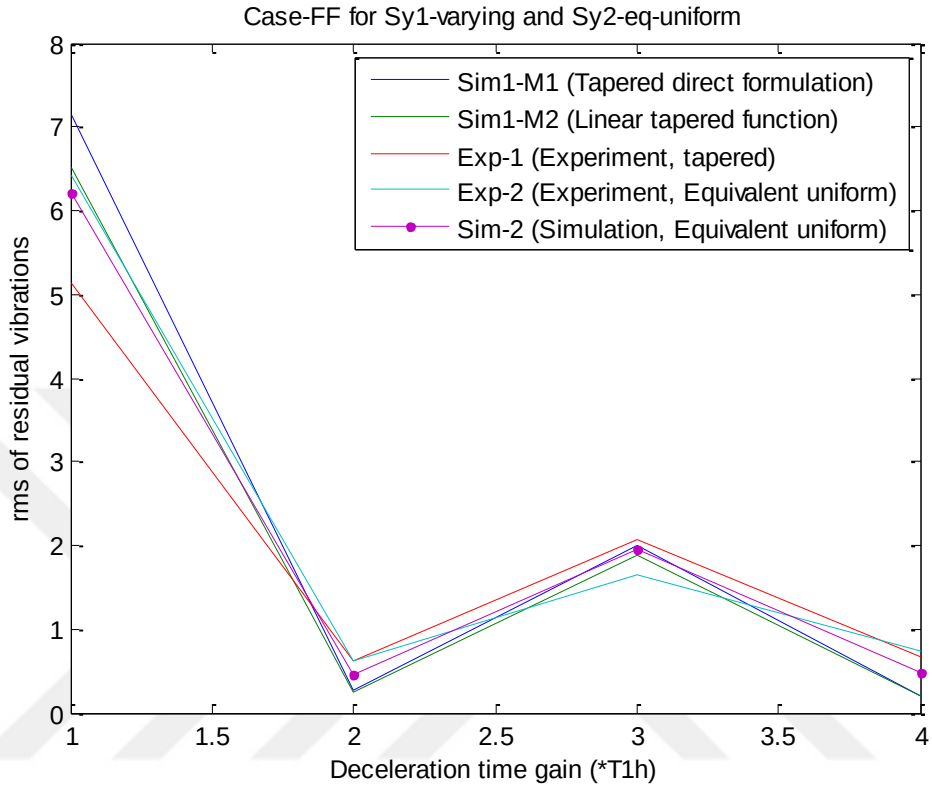

Figure 5.21The comparing Case-FF

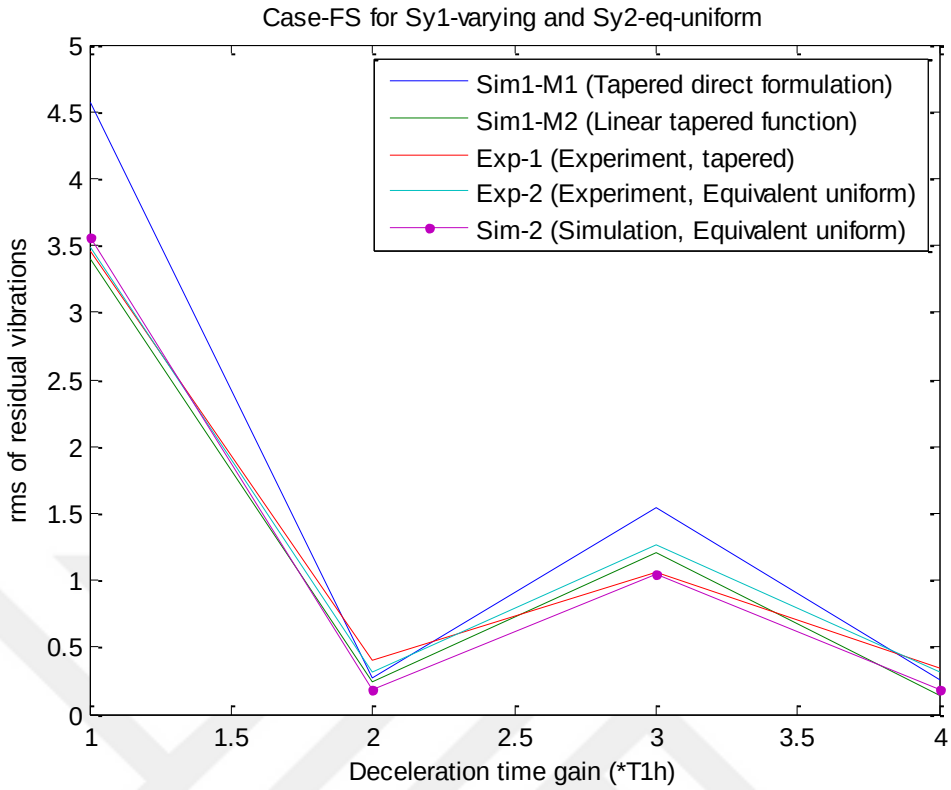

Figure 5.22 The comparing Case-FS

5.4.6 The Cases for tm=2 seconds

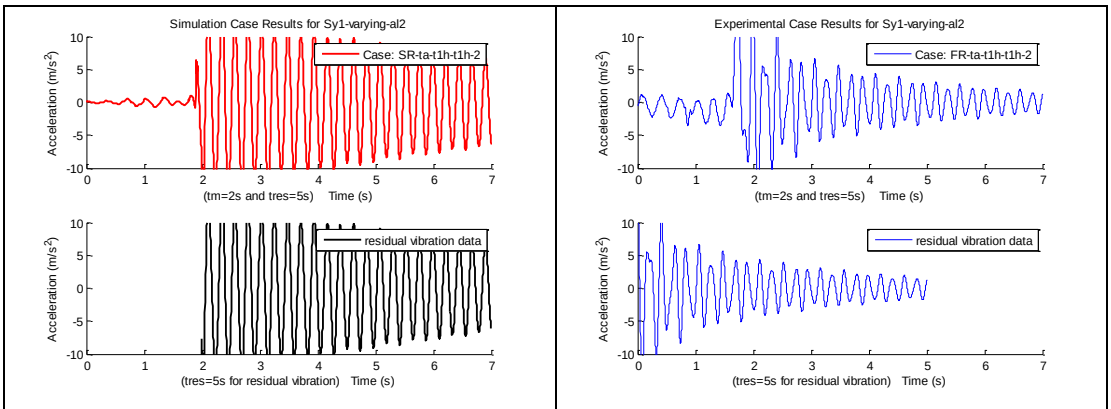

Matlab simulation Sim1-M2 RMS for the residual is 7.1097	Experiment RMS for the residual is 3.3726

Figure 5.23 CASE FR-1 (tm=2s, tres=5s)

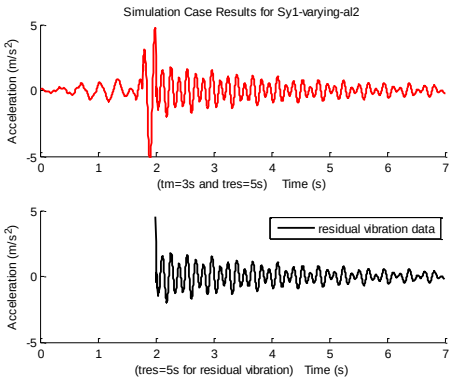	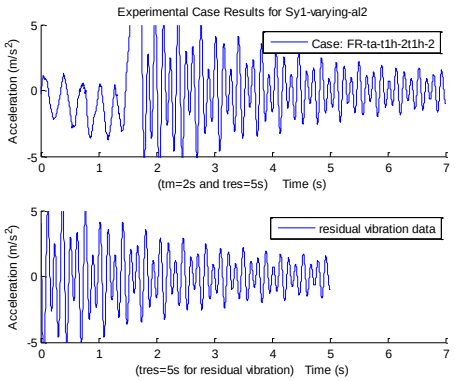
Matlab simulation Sim1-M2 RMS for the residual is 0.6377	Experiment RMS for the residual is 1.9541

Figure 5.24 CASE FR-2 (tm=2s, tres=5s)

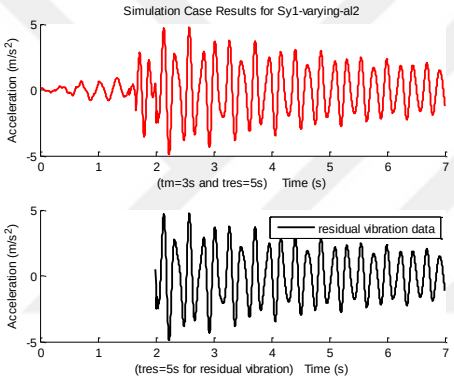	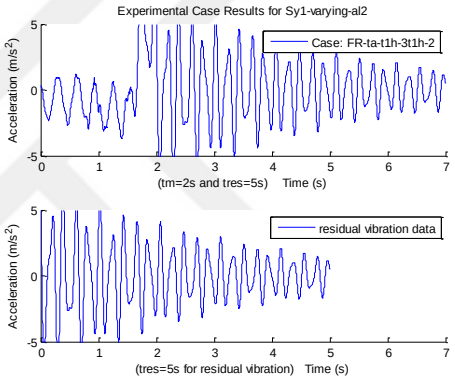
Matlab simulation Sim1-M2 RMS for the residual is 1.9613	Experiment RMS for the residual is 2.3630

Figure 5.25 CASE FR-3 (tm=2s, tres=5s)

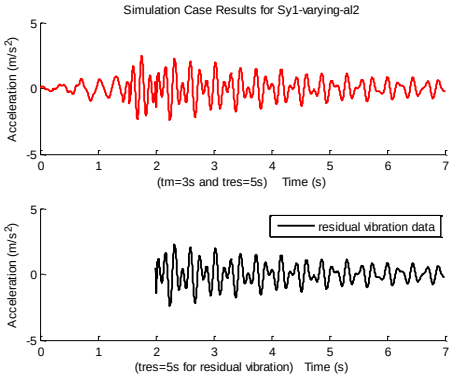	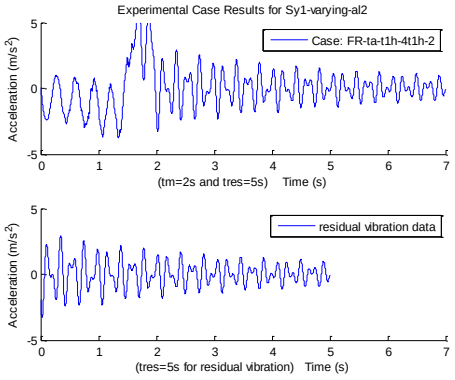
Matlab simulation RMS is 0.7835	Experiment RMS for the residual is 0.9847

Figure 5.26 CASE FR-4 (tm=2s, tres=5s)

Analyzing the rms results of the motion inputs of the case, it is observed that the even multiples of the t1h parameter have more effective reduction compared to odd multiples of t1h. It is observed that the residual vibration levels are high for td=t1h, and residual vibration levels are significantly decreased for td=2t1h. The rms results are shown in Table 5.11.

Table 5.11 The rms values for residual vibrations for motion time is 2 seconds.

tm=2s. sy1_varying_al2	Exp-1	Sim1-M2
Case fr-1 tm=2s	3.3726	7.1097
Case fr-2 tm=2s	1.9541	0.6377
Case fr-3 tm=2s	2.3630	1.9613
Case fr-4 tm=2s	0.9847	0.7835

5.5 System Sy3_varying_al2

The considered manipulator system is shown in Figure 5.27. The manipulator links have linearly tapered beams.

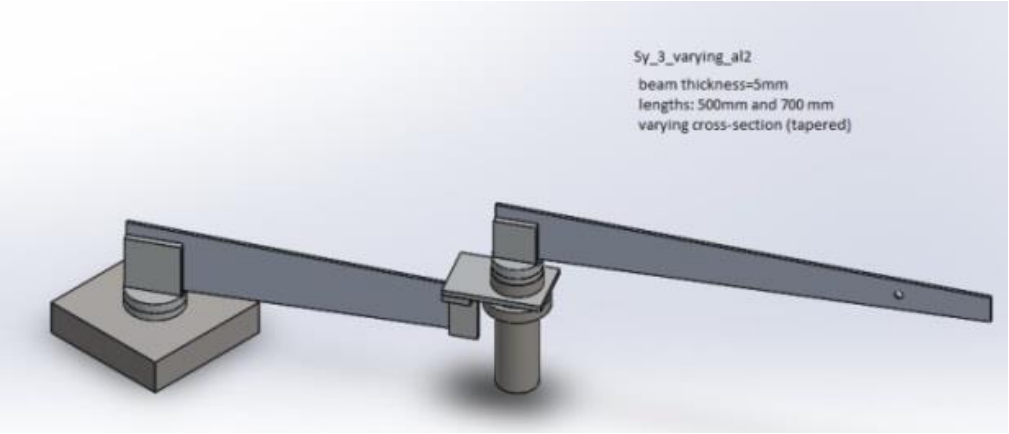

Figure 5.27 The Sy3-varying-al2

Table 5.12 The Sy3_varying_al2

Position		ϕ_{2s}	ϕ_{3s}	Sim3-M2 f_1 (Hz)	Exp-3
Position	Pictorial				
Pos-f	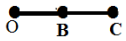	0^o	0^o	2.5849	2.5608
Pos-s	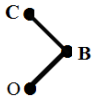	45^o	90^o	2.8423	2.7867
Pos-r		90^o	170^o	3.1754 * 2.9346	3.2386 *3.0880
*: with tip mass (400gr)					

Table 5.13 The RMS values of Case-FF of Sy3_varying_al2

sy3_varying_al2 Without payload	Exp-3	Sim3-M2
Case FF-1 tm=3s	7.3944	7.1736
Case FF-2 tm=3s	0.6380	0.6802
Case FF-3 tm=3s	2.4954	2.1934
Case FF-4 tm=3s	0.69	0.5569

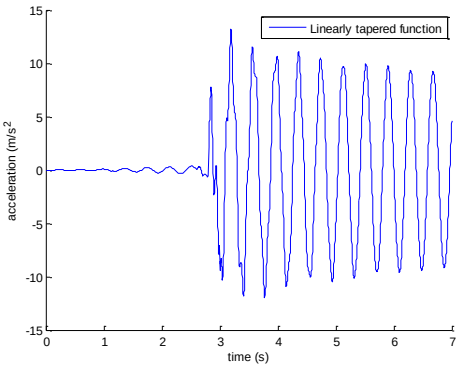

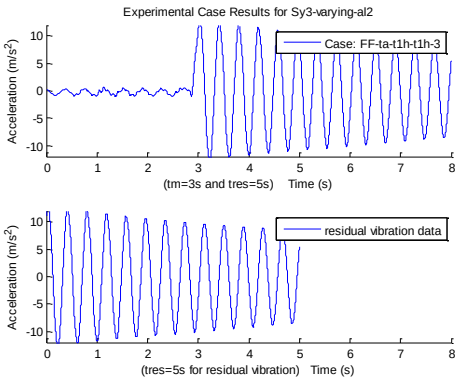

Matlab simulation RMS=7.1736	Experiment. RMS for the residual is 7.3944

Figure 5.27 CASE FF-1 (tm=3s, tres=5s)

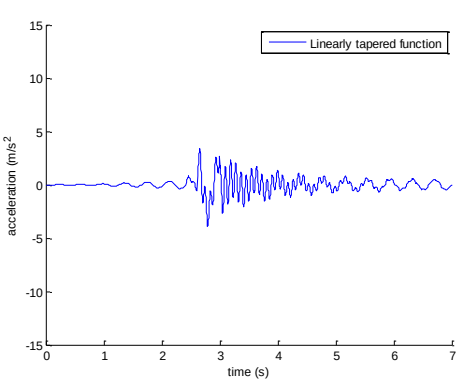

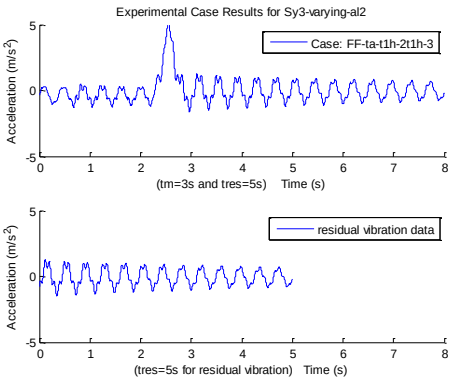

Matlab simulation Sim1-M2 RMS=0.6802	Experiment. RMS for the residual is 0.6380

Figure 5.28 CASE FF-2 (tm=3s, tres=5s)

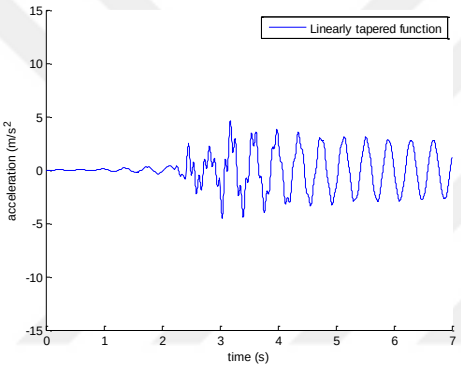

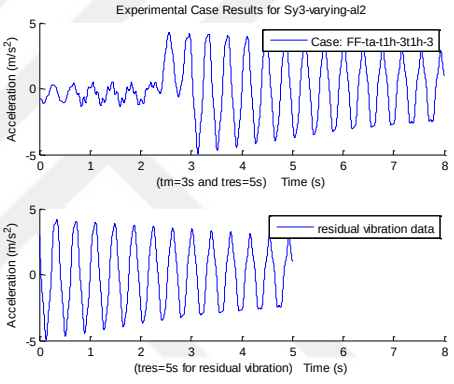

Matlab simulation RMS=2.1934	Experiment. RMS for the residual is 2.4954

Figure 5.29 CASE FF-3 (tm=3s, tres=5s)

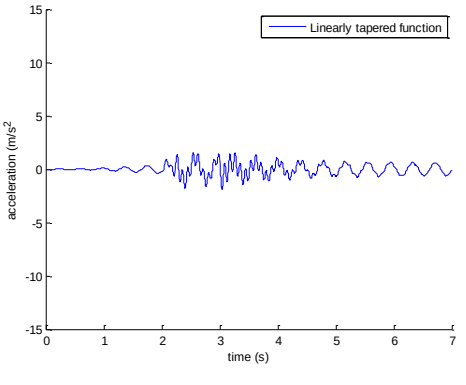

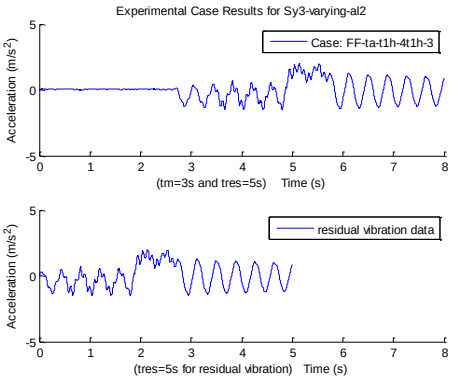

Matlab simulation Sim1-M2 RMS= 0.5569	Experiment.RMS for the residual is 0.69

Figure 5.30 CASE FF-4 (tm=3s, tres=5s)

The rms graphics for Case-ff of the Sy3-varying-al2 is shown in Figure 5.31. Analyzing the rms results of the motion inputs of the case, it is observed that the even multiples of the t1h parameter have more effective reduction compared to odd multiples of t1h.

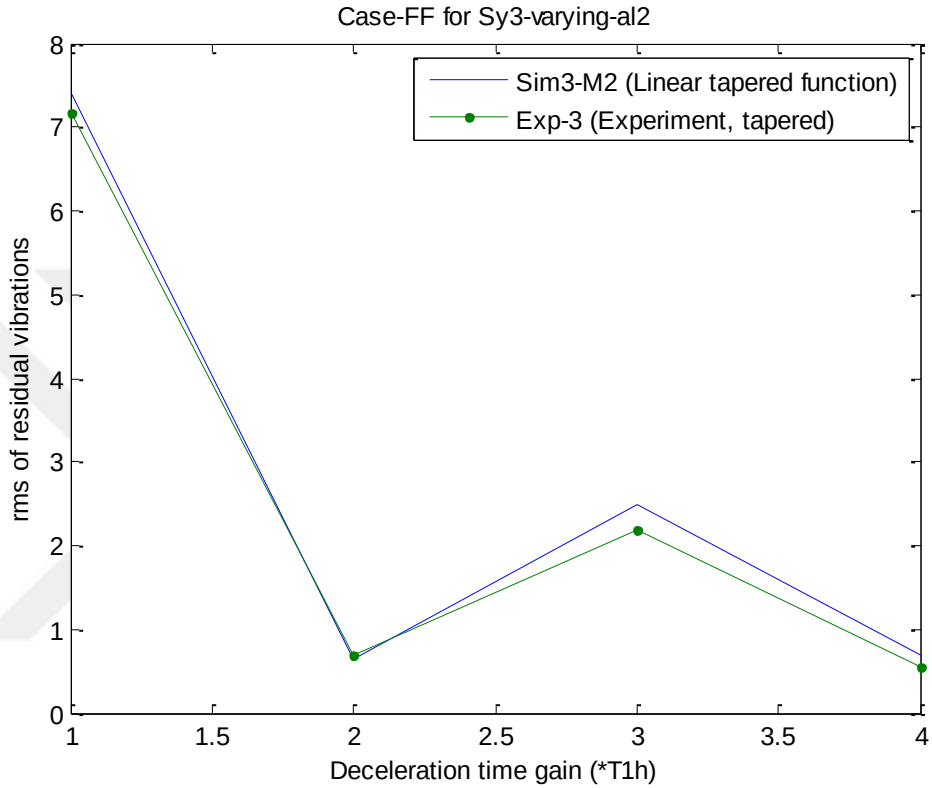

Figure 5.31 The rms graphic of case-ff for Sy3-varying-al2

CHAPTER EIGHT
CONCLUSION

In this thesis, two-link planar robot manipulator configurations with linearly tapered beams are considered. The manipulators have flexible joints and flexible links. In the studies, the end point vibration signals are simulated by developing a MatLAB code based on the finite element theory and Newmark numerical integration. Also, experimental results have been obtained for different manipulator systems. Trapezoidal velocity profiles for the actuating motors have been used. Various starting and stopping positions for the end point are studied with various trapezoidal motion profiles.

The idea of the choosing a suitable deceleration time based on the natural frequency is extended to the two-link flexible manipulators with linearly tapered beams. The natural frequency of the two-link manipulator system change as it moves. It is observed that the deceleration time of the trapezoidal velocity profile based on the natural frequency of the two-link robot manipulator configurations at the stopping point is important for suppressing the residual vibrations. The comparison of the simulation obtained with the developed MatLAB codes and experimental results show that they are in good agreement. It is observed that the passive control methodology has been applicable to manipulators systems which have two and more degree of freedom systems

The results obtained in this study support that the proposed method can be used in practice, especially in pick and place applications to control residual vibrations. The modeling procedure can be used for the dynamic analysis of multi-body flexible systems such as multi-link serial robots.

This modeling procedure and the proposed control approach can be extended to dynamic vibration analysis and control on more complex and composite structures.

REFERENCES

Abe, A. (2009). Trajectory planning for residual vibration suppression of a two-link rigid-flexible manipulator considering large deformation. *Mechanism and Machine Theory, 44*, 1627–1639.

Ankarali, A., & Diken, H. (1997). Vibration control of an elastic manipulator link. *Journal of Sound and Vibration, 204*(1), 162-170.

Bathe, K.J. (2014). *Finite element procedures*, (2nd Edition). New Jersey: Prentice-Hall.

Bayat, M. (2011). Analytical study on the vibration frequencies of tapered beams. *Latin America journal of solid and structure*. 8, 149 -162.

Benosman, M., & LeVey, G. (2004). Control of flexible manipulators: a survey. *Robotica, 22*, 533-545.

Dwivedy, S.K., & Eberhard, P. (2006). Dynamic analysis of flexible manipulators, a literature review. *Mechanism and Machine Theory, 41*, 749-777.

Friedman, Z., Kosmatka, J.B. (1992). Exact Stiffness matrix of a nonuniform Beam-I. Extension, Torsion, and Bending of a Bernoulli-Euler Beam. *Computers & Structures, 42*, 671-682.

Fung, T.C. (1997). Unconditionally stable higher-order Newmark methods by sub-stepping procedure. *Computer Methods in Applied Mechanics and Engineerin,147*, 61-84.

Green, A., & Sasiadek, J.Z. (2004). Dynamics and trajectory tracking control of a two-link robot manipulator. *Journal of Vibration and Control, 10,* 1415–1440.

Gurses, K. Bradley, J.B., & Edward, J.P. (2009).Vibration control of a single-link flexible manipulator using an array of fiber optic curvature sensors and PZT actuators. *Mechatronics,19*, 167–177.

Karagulle, H., & Malgaca, L. (2004). Analysis of end point vibrations of a two-link manipulator by integrated CAD/CAE procedures. *Finite Elements in Analysis and Design, 40*, 2049-2061.

Mimmi, G., & Pennacchi, P. (2001). Pre-shaping motion input for a rotating flexible link. *International Journal of Solids and Structures, 38*, 2009-2023.

Mirzaee, E.Eghtesad, M., &Fazelzadeh, S.A. (2010). Maneuver control and active vibration suppression of a two-link flexible arm using a hybrid variable structure/Lyapunov control design. *Acta Astronautica, 67*, 1218–1232.

Newmark, N.M. (1959). A method of computation for structural dynamics. *Journal of Engineering Mechanics, ASCE 85*, 67-94.

Owren, B., & Simonsen, H.H. (1995). Alternative integration methods for problems in structural dynamics. *Computer Methods in Applied Mechanics and Engineering, 122*, 1-10.

Ozer, A., & Semercigil, S.E. (2008). An event-based vibration control for a two-link flexible robotic arm: numerical and experimental observations. *Journal of Sound and Vibration, 313*, 375–394.

Park, K.J. (2004). Flexible robot manipulator path design to reduce the endpoint residual vibration under torque constraints. *Journal of Sound and Vibration,*275, 1051–1068.

Shan, J., Liu, H.T., & Sun, S. (2005). Modified input shaping for a rotating single-link flexible manipulator. *Journal of Sound and Vibration,285*, 187–207.

Shin, H.C., & Choi, S.B. (2001). Position control of a two link flexible manipulator featuring piezoelectric actuators and sensors. *Mechatronics, 11,* 707-729.

Shin, K., & Brennan, M.J. (2008). Two simple methods to suppress the residual vibrations of a translating or rotating flexible cantilever beam. *Journal of Sound and Vibration, 312*, 140–150.

Thomson, W.T., & Dahleh, M.D. (1988). *Theory of vibration with applications*, (3rd Edition), New Jersey: Prentice-Hall.

Zhang, L., Zhu, J.W., & Zheng, Z. (1999).The stochastic Newmark algorithm for random analysis of multi-degree-of-freedom nonlinear systems. *Computers and Structures, 70,* 557-568.

APPENDICES

A1. The MatLAB Codes For FEM Model-1 of The Two-link Manipulator with Linearly Tapered Beams

```
%-----------------------------------------------------------
%% TAPERED FEM MODEL FOR THE SY1-VARYING-AL2  MODEL-I
%%(Developed by Mehmet DİRİLMİŞ)
% the angles in radian.
clc,clear;close all;

%Case studies
fis2=0*pi/180;fis3=0*pi/180;thm2=90*pi/180;thm3=0*pi/180;t1h=1/2.8461/2;    %Case1:FF
      2.8461
%              fis2=0*pi/180;fis3=0*pi/180;thm2=45*pi/180;thm3=90*pi/180;t1h=1/3.3725/2;
      %Case2:FS   3.3725
%            fis2=0*pi/180;fis3=0*pi/180;thm2=90*pi/180;thm3=170*pi/180;t1h=1/4.3461/2;
      %Case3:FR  4.3461
%       fis2=(45)*pi/180;fis3=(90)*pi/180;thm2=45*pi/180;thm3=80*pi/180;t1h=1/4.3461/2;
      %Case4:SR 4.3461

tconst=t1h; % trapezoidal velocity profile
%tconst=0; % triangular velocity profile
tdecel=1*t1h;tmotion=3;tacel=tmotion-tconst-tdecel;td=tmotion;

wmax2=thm2/(0.5*tacel+tconst+0.5*tdecel);
wmax3=thm3/(0.5*tacel+tconst+0.5*tdecel);
dt=0.0025;tson=td+4;
%---------------------
%f0=1/dt;
alphad=0;betad=0.00038;
gama=0.005;
%---
```

```
ne2=20;ne3=40;
%ne2=927;ne3=575;
nel=ne2+ne3;nb=3*nel+2;nf=nb-2;
l2=0.4635;
l3=0.575;
dsensor=0.085;
he2=l2/ne2;he3=l3/ne3;
v1=round(dsensor/he3);nf2=nb-v1*3-2;dshata=dsensor-v1*he3
elm=71e9;ro=2700;
m2=3.2553409;ig2=0.0134189;   %
m3=0.4002648;ig3=0.0000938;   %
kmot2=16000;   % flexible joint
%kmot2=1e10;   % rigid joint
kmot3=kmot2;
%%% 80=(100+60)/2
%%% 60=(80+40)/2
l2_b1=0.100;l2_b2=0.060;  %  (link2) 1.tapered beam için b1 ve b2 yükseklik değerleri
l3_b1=0.080;l3_b2=0.040; % (link3) 2.tapered beam için b1 ve b2 yükseklik değerleri
be2_d=(l2_b1-l2_b2)/(ne2); %
b1_nodes=l2_b1:-be2_d:l2_b2;
fark2=(be2_d)/2;
be3_d=(l3_b1-l3_b2)/(ne3);
fark3=(be3_d)/2;  %


%-----------------------------------------------------------------
th2=fis2;th3=fis2+fis3;
c2=cos(th2);s2=sin(th2);
c3=cos(th3);s3=sin(th3);
;yb1=l2*s2;xc1=xb1+l3*c3;yc1=yb1+l3*s3;
%---
%%% 1.tapered beam için değişkenler tanımlanıyor
l2_b1=l2_b1-fark2;
for k=1:1:ne2;
    b=(l2_b1)-(be2_d)*(k-1);
```

```
    width=0.006;a2=b*width;iz2=b*width^3/12;
    dm2(k)=he2*a2*ro;
  ae(1,k)=a2;ize(1,k)=iz2;he(1,k)=he2;
end

%%% 2.tapered beam için değişkenler tanımlanıyor
l3_b1=l3_b1-fark3;
for k=ne2+1:1:nel;
    b=(l3_b1)-(be3_d)*(k-ne2-1);
    width=0.006;a3=b*width;iz3=b*width^3/12;
    dm3(k)=he3*a3*ro;
   ae(1,k)=a3;ize(1,k)=iz3;he(1,k)=he3;
end
nn=3*nel+2;de(1,1:6)=[nn+1,nn+2,1,2,3,4];nn=2;
for k=2:1:ne2;
   for j=1:1:6;de(k,j)=nn;nn=nn+1;end
   nn=nn-3;
end
nn=3*ne2-1;de(ne2+1,1:6)=[nn,nn+1,nn+3,nn+4,nn+5,nn+6];nn=nn+4;
for k=ne2+2:1:nel;
   for j=1:1:6;de(k,j)=nn;nn=nn+1;end
   nn=nn-3;
end
%de
an0;
%-------------------------------------------------
t=0:dt:tson;ns=length(t);
%---
th2=fis2;th3=fis2+fis3;   %radian
c2=cos(th2);s2=sin(th2);c3=cos(th3);s3=sin(th3);   %radian
uxr(1)=l2*c2+l3*c3;uyr(1)=l2*s2+l3*s3;   %radian
vth2(1)=0;vth3(1)=0;vw2(1)=0;vw3(1)=0;val2(1)=0;val3(1)=0;
for ni=2:1:ns;
  ti=t(ni);
  thm=thm2;w0=wmax2;velti;th2=fis2+th;w2=w;al2=al;
```

```
  thm=thm3;w0=wmax3;velti;th3=th2+fis3+th;w3=w2+w;al3=al2+al;
  vth2(ni)=th2-fis2;vth3(ni)=th3-th2-fis3;
  vw2(ni)=w2;vw3(ni)=w3-w2;
  val2(ni)=al2;val3(ni)=al3-al2;
  c2=cos(th2);s2=sin(th2);c3=cos(th3);s3=sin(th3);
  uxr(ni)=l2*c2+l3*c3;uyr(ni)=l2*s2+l3*s3;
end
uxr=uxr-uxr(1);uyr=uyr-uyr(1);
%----------------------------
fid2=fopen('w2.txt','w');fid3=fopen('w3.txt','w');
for ni=1:1:ns;
 theta2(ni)=vth2(ni);theta3(ni)=vth3(ni);
 v2(ni)=vw2(ni);v3(ni)=vw3(ni);
 acc_a2(ni)=val2(ni);acc_a3(ni)=val3(ni);
 trs_w2=[t(ni);v2(ni);];fprintf(fid2,'%12.5f %12.5f \r\n',trs_w2);
 trs_w3=[t(ni);v3(ni);];fprintf(fid3,'%12.5f %12.5f \r\n',trs_w3);
end
fclose(fid2);fclose(fid3);
%  plot(t,theta2,t,v2,t,acc_a2),pause,
%  plot(t,theta3,t,v3,t,acc_a3),


.........................
ae1=area*elm/h;ei1=elm*iz/h/h/h;
ke=[ae1,0,0,-ae1,0,0
  0,12*ei1,6*ei1*h,0,-12*ei1,6*ei1*h
  0,6*ei1*h,4*ei1*h*h,0,-6*ei1*h,2*ei1*h*h
  -ae1,0,0,ae1,0,0
  0,-12*ei1,-6*ei1*h,0,12*ei1,-6*ei1*h
  0,6*ei1*h,2*ei1*h*h,0,-6*ei1*h,4*ei1*h*h];
me=[140,0,0,70,0,0
  0,156,22*h,0,54,-13*h
  0,22*h,4*h*h,0,13*h,-3*h*h
  70,0,0,140,0,0
  0,54,13*h,0,156,-22*h
  0,-13*h,-3*h*h,0,-22*h,4*h*h]*ro*area*h/420;
```

```
c=cos(th);s=sin(th);
tr=[c,s,0,0,0,0
  -s,c,0,0,0,0
  0,0,1,0,0,0
  0,0,0,c,s,0
  0,0,0,-s,c,0
  0,0,0,0,0,1];
tr1=transpose(tr);kse=tr1*ke*tr;mse=tr1*me*tr;

ms=zeros(nb,nb);cs=zeros(nb,nb);ks=zeros(nb,nb);fs=zeros(nb,1);
for k=1:1:ne2;the(1,k)=th2;end
for k=ne2+1:1:nel;the(1,k)=th3;end
%---
for iel=1:nel;
  area=ae(iel);iz=ize(iel);
  th=the(iel);h=he(iel);fe_elem;
  for n=1:6;
    for m=1:6;
      n1=de(iel,n);
      if n1<=nb;
        n2=de(iel,m);
        if n2<=nb;
        ks(n1,n2)=ks(n1,n2)+kse(n,m);
        ms(n1,n2)=ms(n1,n2)+mse(n,m);
        end
      end
    end
  end
end
n=3*(ne2-
      1)+2;ms(n,n)=ms(n,n)+m2;n=n+1;ms(n,n)=ms(n,n)+m2;n=n+1;ms(n,n)=ms(n,n)+ig2;
n=3*(nel-
      1)+3;ms(n,n)=ms(n,n)+m3;n=n+1;ms(n,n)=ms(n,n)+m3;n=n+1;ms(n,n)=ms(n,n)+ig3;
ks(1,1)=ks(1,1)+kmot2;nn=ne2*3+1;ks(nn,nn)=ks(nn,nn)+kmot3;ks(nn,nn+1)=ks(nn,nn+1)-
      kmot3;
```

```
ks(nn+1,nn+1)=ks(nn+1,nn+1)+kmot3;ks(nn+1,nn)=ks(nn+1,nn)-kmot3;
%---
cs=alphad*ms+betad*ks;

ww2=w2;aal2=al2;fs=zeros(nb,1);
re=0.5*he2;aex=-re*ww2^2*c2-re*aal2*s2;aey=-re*ww2^2*s2+re*aal2*c2;
%qx=-dm2*(c2*aex+s2*aey);qy=-dm2*(-s2*aex+c2*aey);
qx=-dm2(1)*aex;qy=-dm2(1)*aey;qyt=-dm2(1)*(-s2*aex+c2*aey);  %% dm2 değişken
    olacak,
%qx=-dm2*aex;qy=-dm2*aey;qyt=-dm2*(-s2*aex+c2*aey);
fs(1,1)=qyt*he2/12;fs(2,1)=qx/2;fs(3)=qy/2;fs(4,1)=qyt*he2/12;kk=2;
for k=2:1:ne2;
  re=0.5*(2*k-1)*he2;aex=-re*ww2^2*c2-re*aal2*s2;aey=-re*ww2^2*s2+re*aal2*c2;
  qx=-dm2(k)*aex;qy=-dm2(k)*aey;qyt=-dm2(k)*(-s2*aex+c2*aey);
  fs(kk)=fs(kk)+qx/2;fs(kk+1)=fs(kk+1)+qy/2;fs(kk+2)=fs(kk+2)+qyt*he2/12;
  kk=kk+3;fs(kk)=fs(kk)+qx/2;fs(kk+1)=fs(kk+1)+qy/2;fs(kk+2)=fs(kk+2)+qyt*he2/12;
end
re=l2;abx=-re*ww2^2*c2-re*aal2*s2;aby=-re*ww2^2*s2+re*aal2*c2;
fs(kk)=fs(kk)-m2*abx;fs(kk+1)=fs(kk+1)-m2*aby;fs(kk+2)=fs(kk+2)-ig2*aal2;
%---------------
ww3=w3;aal3=al3;
re=0.5*he3;aex=abx-re*ww3^2*c3-re*aal3*s3;aey=aby-re*ww3^2*s3+re*aal3*c3;
qx=-dm3(ne2+1)*aex;qy=-dm3(ne2+1)*aey;qyt=-dm3(ne2+1)*(-s3*aex+c3*aey);
fs(kk,1)=fs(kk,1)+qx/2;fs(kk+1,1)=fs(kk+1,1)+qy/2;fs(kk+3,1)=fs(kk+3,1)+qyt*he3/12;
kk=kk+4;fs(kk,1)=fs(kk,1)+qx/2;fs(kk+1,1)=fs(kk+1,1)+qy/2;fs(kk+2,1)=fs(kk+2,1)+qyt*he
    3/12;
for k=2:1:ne3;
  re=0.5*(2*k-1)*he3;aex=abx-re*ww3^2*c3-re*aal3*s3;aey=aby-
      re*ww3^2*s3+re*aal3*c3;
  qx=-dm3(ne2+k)*aex;qy=-dm3(ne2+k)*aey;qyt=-dm3(ne2+k)*(-s3*aex+c3*aey);
  fs(kk,1)=fs(kk,1)+qx/2;fs(kk+1,1)=fs(kk+1,1)+qy/2;fs(kk+2,1)=fs(kk+2,1)+qyt*he2/12;

      kk=kk+3;fs(kk,1)=fs(kk,1)+qx/2;fs(kk+1,1)=fs(kk+1,1)+qy/2;fs(kk+2,1)=fs(kk+2,1)+q
      yt*he2/12;
end
```

```
re=l3;aex=abx-re*ww3^2*c3-re*aal3*s3;aby=-re*ww3^2*s3+re*aal3*c3;
fs(kk,1)=fs(kk,1)-m3*aex;fs(kk+1,1)=fs(kk+1,1)-m3*aey;fs(kk+2,1)=fs(kk+2,1)-ig3*aal3;

an0;fe_model;ms1=inv(ms);
line([0,xb1,xc1],[0,yb1,yc1]),axis equal square
[p,s]=eig(-ms1*ks);wn=diag(sqrt(s));fn=wn/(2*pi);
fnl=imag(sort(fn));
f1_initial=vpa(fnl(1:5),8)  % the first 5 natural frequency
mu=transpose(p)*ms*p;
ku=transpose(p)*ks*p;

w0=thm/(0.5*tacel+tconst+0.5*tdecel);
if ti<tacel;
  th=w0*ti^2/(2*tacel);w=w0*ti/tacel;al=w0/tacel;
elseif ti<=td-tdecel;
  th=w0*tacel/2+w0*(ti-tacel);w=w0;al=0;
elseif ti<td;
  th=thm-w0*(td-ti)^2/(2*tdecel);w=w0*(td-ti)/tdecel;al=-w0/tdecel;
else
  w=0;th=thm;al=0;
end

%---Newmark integration
alpha=0.25*(1+gama)^2;delta=0.5+gama;
a0=1/(alpha*dt^2);a1=delta/(alpha*dt);
a2=1/(alpha*dt);a3=1/(2*alpha)-1;
a4=delta/alpha-1;a5=(dt/2)*(delta/alpha-2);
a6=dt*(1-delta);a7=delta*dt;
t=0:dt:tson;ns=length(t);
u(1:nb,1:ns)=0;u1(1:nb,1:ns)=0;u2(1:nb,1:ns)=0;
%---
  ti=t(ni);
  thm=thm2;w0=wmax2;velti;th2=fis2+th;w2=w;al2=al;
  thm=thm3;w0=wmax3;velti;th3=th2+fis3+th;w3=w2+w;al3=al2+al;
  c2=cos(th2);s2=sin(th2);c3=cos(th3);s3=sin(th3);
```

```
  up=u(1:nb,ni-1);u1p=u1(1:nb,ni-1);u2p=u2(1:nb,ni-1);
  uc=fs+ms*(a0*up+a2*u1p+a3*u2p)+cs*(a1*up+a4*u1p+a5*u2p);uc=mat1*uc;
  u2c=a0*(uc-up)-a2*u1p-a3*u2p;
  u1c=u1p+a6*u2p+a7*u2c;
  u(1:nb,ni)=uc;u1(1:nb,ni)=u1c;u2(1:nb,ni)=u2c;
end
nf=nf2;
ux=u(nf,1:ns);uy=u(nf+1,1:ns);usum=sqrt(ux.^2+uy.^2); %displacement (m)
ux1=u1(nf,1:ns);uy1=u1(nf+1,1:ns); %velocity
ux2=u2(nf,1:ns);uy2=u2(nf+1,1:ns); %acceleration

fi=fis2+thm2+fis3+thm3+pi/2;c=cos(fi);s=sin(fi);
ud=ux*c+uy*s;ud1=ux1*c+uy1*s;ud2=ux2*c+uy2*s;
%plot(t,uy)  % y-axes deflection (m); pause
axis([0 7 -15 15]),hold on,plot(t,ud2),xlabel('time (s)'),ylabel('acceleration
    (m/s^2'),legend('Equivalent tapered')
ns1=round(tmotion/dt);ns2=round(tson/dt);
t1=t(ns1:ns2);y1=ud2(ns1:ns2);
yrms=sqrt(mean(y1.^2)),
return
%ux=uxr+ux;uy=uyr+uy;
%plot(t,uyr,t,uy)
%plot2


% %%%
% figure
% plot(x,y)
% axis([-1.2 1.2 -1.2 1.2])
% axis equal square
% title('axis([-1.2 1.2 -1.2 1.2]); axis square')
```

A2. The MatLAB Codes For FEM Model-2 of The Two-link Manipulator with Linearly Tapered Beams

```
%-----------------------------------------------------------
%% TAPERED FEM MODEL FOR THE SY1-VARYING-AL2 using varying function MODEL-II
%%(Developed by Mehmet DİRİLMİŞ)
% the angles in radian.

clc,clear;close all;
%Case studies
%fis2=0*pi/180;fis3=0*pi/180;thm2=90*pi/180;thm3=0*pi/180;t1h=1/2.8706/2;
%Case1:FF   2.8706132
%fis2=0*pi/180;fis3=0*pi/180;thm2=45*pi/180;thm3=90*pi/180;t1h=1/3.4033/2;
%Case2:FS   3.4033
fis2=0*pi/180;fis3=0*pi/180;thm2=90*pi/180;thm3=170*pi/180;t1h=1/4.3909/2;
%Case3:FR   4.3909
%fis2=(45)*pi/180;fis3=(90)*pi/180;thm2=45*pi/180;thm3=80*pi/180;t1h=1/4.3909/2;
%Case4:SR  4.3909

tconst=t1h; % trapezoidal velocity profile
%tconst=0; % triangular velocity profile
tdecel=1*t1h;
tmotion=2;   % tmotion=3;
tacel=tmotion-tconst-tdecel;td=tmotion;

wmax2=thm2/(0.5*tacel+tconst+0.5*tdecel);
wmax3=thm3/(0.5*tacel+tconst+0.5*tdecel);
```

```
dt=0.0025;tson=td+5;
%---------------------
%f0=1/dt;
alphad=0;betad=0.00038;
gama=0.005;
%---
ne2=20;ne3=40;
%ne2=4;ne3=6;
%ne2=927;ne3=575;
nel=ne2+ne3;nb=3*nel+2;nf=nb-2;
l2=0.4635;
l3=0.575;
dsensor=0.085;
he2=l2/ne2;he3=l3/ne3;
v1=round(dsensor/he3);nf2=nb-v1*3-2;dshata=dsensor-v1*he3
elm=71e9;ro=2700;
m2=3.2553409;ig2=0.0134189;   % motor2 point mass
m3=0.4002648;ig3=0.0000938;   % payload point mass
kmot2=16000;   % flexible joint
%kmot2=1e10;   % rigid joint
kmot3=kmot2;
%%% 80=(100+60)/2
%%% 60=(80+40)/2
l2_b1=0.100;l2_b2=0.060;  %  (link2) 1.tapered beam için b1 ve b2 yükseklik değerleri
l3_b1=0.080;l3_b2=0.040; % (link3) 2.tapered beam için b1 ve b2 yükseklik değerleri
be2_d=(l2_b1-l2_b2)/(ne2);
```

```
be3_d=(l3_b1-l3_b2)/(ne3); %
%%% ağırlık merkezi
re21=(he2/3)*[(l2_b1+2*(l2_b1-be2_d))/(l2_b1+(l2_b1-be2_d))];re22=he2-re21;
re31=(he3/3)*[(l3_b1+2*(l3_b1-be3_d))/(l3_b1+(l3_b1-be3_d))];re32=he3-re31;

%%%b1=l2_b1;b2=l2_b1-be2_d;
%---------------------------------------------------------------
th2=fis2;th3=fis2+fis3;
c2=cos(th2);s2=sin(th2);
c3=cos(th3);s3=sin(th3);
xb1=l2*c2;yb1=l2*s2;xc1=xb1+l3*c3;yc1=yb1+l3*s3;
%---
%%% 1.tapered beam için değişkenler tanımlanıyor

for k=1:1:ne2;
    b=(l2_b1)-(be2_d)*(k-1);b1=b;b2=b-be2_d;%b2=b;
  %% alfa(k)=(l2_b2-l2_b1)/l2_b1;  % if alfa=0 then the matrixes are for uniform beam.
  %alfa(k)=(b2-b1)/b1
  %alfa(k)=(b2-b1)/b1
  tanalfa=((l2_b1-l2_b2)/2)/l2;
  ccc=2*he2*tanalfa/b;
%    ccc(k)=(b2-b1)/b1;
    %% h yerine width yazıldı. width=6mm constant.
    width=0.006;a2=b*width;iz2=b*width^3/12;
    dm2(k)=he2*a2*ro;
  ae(1,k)=a2;ize(1,k)=iz2;he(1,k)=he2;
```

```
end

%%% 2.tapered beam için değişkenler tanımlanıyor
for k=ne2+1:1:nel;
     b=(l3_b1)-(be3_d)*(k-ne2-1);b1=b;b2=b-be3_d;%b2=b;
%alfa(k)=(l3_b2-l3_b1)/l3_b1;
%alfa(k)=(b2-b1)/b1;
tanalfa=((l3_b1-l3_b2)/2)/l3;
ccc=2*he3*tanalfa/b;
%      ccc(k)=(b2-b1)/b1;
     width=0.006;a3=b*width;iz3=b*width^3/12;
     dm3(k)=he3*a3*ro;
   ae(1,k)=a3;ize(1,k)=iz3;he(1,k)=he3;
end
nn=3*nel+2;de(1,1:6)=[nn+1,nn+2,1,2,3,4];nn=2;
   for j=1:1:6;de(k,j)=nn;nn=nn+1;end
   nn=nn-3;
end
nn=3*ne2-1;de(ne2+1,1:6)=[nn,nn+1,nn+3,nn+4,nn+5,nn+6];nn=nn+4;
for k=ne2+2:1:nel;
   for j=1:1:6;de(k,j)=nn;nn=nn+1;end
   nn=nn-3;
end
de;

%--------------------------------------------------
```

```
t=0:dt:tson;ns=length(t);
%---
th2=fis2;th3=fis2+fis3;   %radian
c2=cos(th2);s2=sin(th2);c3=cos(th3);s3=sin(th3);   %radian
uxr(1)=l2*c2+l3*c3;uyr(1)=l2*s2+l3*s3;   %radian
vth2(1)=0;vth3(1)=0;vw2(1)=0;vw3(1)=0;val2(1)=0;val3(1)=0;
for ni=2:1:ns;
  ti=t(ni);
  thm=thm2;w0=wmax2;velti;th2=fis2+th;w2=w;al2=al;
  thm=thm3;w0=wmax3;velti;th3=th2+fis3+th;w3=w2+w;al3=al2+al;
  vth2(ni)=th2-fis2;vth3(ni)=th3-th2-fis3;
  vw2(ni)=w2;vw3(ni)=w3-w2;
  val2(ni)=al2;val3(ni)=al3-al2;
  c2=cos(th2);s2=sin(th2);c3=cos(th3);s3=sin(th3);
  uxr(ni)=l2*c2+l3*c3;uyr(ni)=l2*s2+l3*s3;
end
uxr=uxr-uxr(1);uyr=uyr-uyr(1);
%----------------------------
fid2=fopen('w2.txt','w');fid3=fopen('w3.txt','w');
for ni=1:1:ns;
 theta2(ni)=vth2(ni);theta3(ni)=vth3(ni);
 v2(ni)=vw2(ni);v3(ni)=vw3(ni);
 acc_a2(ni)=val2(ni);acc_a3(ni)=val3(ni);
 trs_w2=[t(ni);v2(ni);];fprintf(fid2,'%12.5f %12.5f \r\n',trs_w2);
 trs_w3=[t(ni);v3(ni);];fprintf(fid3,'%12.5f %12.5f \r\n',trs_w3);
fclose(fid2);fclose(fid3);
```

```
%  plot(t,theta2,t,v2,t,acc_a2),pause,
%  plot(t,theta3,t,v3,t,acc_a3)

KM1=(elm*area/h)*[ccc/log(ccc+1)];
KM2=(elm*iz/h^3)*[2*ccc^2*log(ccc+1)/((ccc+2)*log(ccc+1)-2*ccc)];
KM3=(elm*iz/h^2)*[(2*ccc*(ccc-log(ccc+1)))/((ccc+2)*log(ccc+1)-2*ccc)];
KM4=(elm*iz/h)*[(2*log(ccc+1)+ccc*(ccc-2))/((ccc+2)*log(ccc+1)-2*ccc)];

ke=[KM1,0,0,-KM1,0,0
  0,KM2,KM3,0,-KM2,KM2*h-KM3
  0,KM3,KM4,0,-KM3,KM3*h-KM4
  -KM1,0,0,KM1,0,0
  0,-KM2,-KM3,0,KM2,KM3-KM2*h
  0,KM2*h-KM3,KM3*h-KM4,0,KM3-KM2*h,KM2*h*h-2*KM3*h+KM4];
%ke1=simplify(ke)
me=[(ccc+4)/12,0,0,(ccc+2)/12,0,0
  0,(3*ccc+13)/35,h*(7*ccc+22)/420,0,9*(ccc+2)/140,-h*(6*ccc+13)/420
  0,h*(7*ccc+22)/420,h*h*(3*ccc+8)/840,0,h*(7*ccc+13)/420,-h*h*(ccc+2)/280
  (ccc+2)/12,0,0,(3*ccc+4)/12,0,0
  0,9*(ccc+2)/140,h*(7*ccc+13)/420,0,(10*ccc+13)/35,-h*(15*ccc+22)/420
  0,-h*(6*ccc+13)/420,-h*h*(ccc+2)/280,0,-
h*(15*ccc+22)/420,h*h*(5*ccc+8)/840]*ro*area*h;
%me1=simplify(me)

c=cos(th);s=sin(th);
tr=[c,s,0,0,0,0
  -s,c,0,0,0,0
  0,0,1,0,0,0
  0,0,0,c,s,0
  0,0,0,-s,c,0
  0,0,0,0,0,1];
tr1=transpose(tr);kse=tr1*ke*tr;mse=tr1*me*tr;

ms=zeros(nb,nb);cs=zeros(nb,nb);ks=zeros(nb,nb);fs=zeros(nb,1);
for k=1:1:ne2;the(1,k)=th2;end
```

```
for k=ne2+1:1:nel;the(1,k)=th3;end
%---
  area=ae(iel);iz=ize(iel);
  th=the(iel);h=he(iel);fe_elem;
  for n=1:6;
    for m=1:6;
      n1=de(iel,n);
      if n1<=nb;
        n2=de(iel,m);
        if n2<=nb;
        ks(n1,n2)=ks(n1,n2)+kse(n,m);
        ms(n1,n2)=ms(n1,n2)+mse(n,m);
        end


re21=(he2/3)*[(l2_b1+2*(l2_b1-be2_d))/(l2_b1+(l2_b1-be2_d))];re22=he2-re21; % x-axes
of center of gravity for the finite element of link2
re31=(he3/3)*[(l3_b1+2*(l3_b1-be3_d))/(l3_b1+(l3_b1-be3_d))];re32=he3-re31; % x-axes
of center of gravity for the finite element of link3


ww2=w2;aal2=al2;fs=zeros(nb,1);
re=re21;
re=re21*he2;aex=-re*ww2^2*c2-re*aal2*s2;aey=-re*ww2^2*s2+re*aal2*c2;
%qx=-dm2*(c2*aex+s2*aey);qy=-dm2*(-s2*aex+c2*aey);
qx=-dm2(1)*aex;qy=-dm2(1)*aey;qyt=-dm2(1)*(-s2*aex+c2*aey);  %% dm2   değişken
%qx=-dm2*aex;qy=-dm2*aey;qyt=-dm2*(-s2*aex+c2*aey);

%%%kats=1/2;
kats1=re22/he2;kats2=re21/he2;
fs(1,1)=qyt*he2/12;fs(2,1)=qx*kats1;fs(3)=qy*kats1;fs(4,1)=qyt*he2/12;kk=2;
%fs(1,1)=qyt*he2/12;fs(2,1)=qx/2;fs(3)=qy/2;fs(4,1)=qyt*he2/12;kk=2;
for k=2:1:ne2;
  re=re21*(2*k-1)*he2;aex=-re*ww2^2*c2-re*aal2*s2;aey=-re*ww2^2*s2+re*aal2*c2;
  qx=-dm2(k)*aex;qy=-dm2(k)*aey;qyt=-dm2(k)*(-s2*aex+c2*aey);
```

```
    % fs(kk)=fs(kk)+qx/2;fs(kk+1)=fs(kk+1)+qy/2;fs(kk+2)=fs(kk+2)+qyt*he2/12;
    % kk=kk+3;fs(kk)=fs(kk)+qx/2;fs(kk+1)=fs(kk+1)+qy/2;fs(kk+2)=fs(kk+2)+qyt*he2/12;
   fs(kk)=fs(kk)+qx*kats2;fs(kk+1)=fs(kk+1)+qy*kats2;fs(kk+2)=fs(kk+2)+qyt*he2/12;

kk=kk+3;fs(kk)=fs(kk)+qx*kats1;fs(kk+1)=fs(kk+1)+qy*kats1;fs(kk+2)=fs(kk+2)+qyt*he2/
12;
end
re=l2;abx=-re*ww2^2*c2-re*aal2*s2;aby=-re*ww2^2*s2+re*aal2*c2;
fs(kk)=fs(kk)-m2*abx;fs(kk+1)=fs(kk+1)-m2*aby;fs(kk+2)=fs(kk+2)-ig2*aal2;
%---------------
ww3=w3;aal3=al3;
re=re31*he3;aex=abx-re*ww3^2*c3-re*aal3*s3;aey=aby-re*ww3^2*s3+re*aal3*c3;
qx=-dm3(ne2+1)*aex;qy=-dm3(ne2+1)*aey;qyt=-dm3(ne2+1)*(-s3*aex+c3*aey);

%fs(kk,1)=fs(kk,1)+qx/2;fs(kk+1,1)=fs(kk+1,1)+qy/2;fs(kk+3,1)=fs(kk+3,1)+qyt*he3/12;
%kk=kk+4;fs(kk,1)=fs(kk,1)+qx/2;fs(kk+1,1)=fs(kk+1,1)+qy/2;fs(kk+2,1)=fs(kk+2,1)+qyt*
he3/12;
kats3=re32/he3;kats4=re31/he3;
fs(kk,1)=fs(kk,1)+qx*kats4;fs(kk+1,1)=fs(kk+1,1)+qy*kats4;fs(kk+3,1)=fs(kk+3,1)+qyt*he
3/12;
kk=kk+4;fs(kk,1)=fs(kk,1)+qx*kats3;fs(kk+1,1)=fs(kk+1,1)+qy*kats3;fs(kk+2,1)=fs(kk+2,1
)+qyt*he3/12;
for k=2:1:ne3;
  re=re31*(2*k-1)*he3;aex=abx-re*ww3^2*c3-re*aal3*s3;aey=aby-
re*ww3^2*s3+re*aal3*c3;
  qx=-dm3(ne2+k)*aex;qy=-dm3(ne2+k)*aey;qyt=-dm3(ne2+k)*(-s3*aex+c3*aey);
%   fs(kk,1)=fs(kk,1)+qx/2;fs(kk+1,1)=fs(kk+1,1)+qy/2;fs(kk+2,1)=fs(kk+2,1)+qyt*he2/12;
%
kk=kk+3;fs(kk,1)=fs(kk,1)+qx/2;fs(kk+1,1)=fs(kk+1,1)+qy/2;fs(kk+2,1)=fs(kk+2,1)+qyt*he
2/12;

fs(kk,1)=fs(kk,1)+qx*kats4;fs(kk+1,1)=fs(kk+1,1)+qy*kats4;fs(kk+2,1)=fs(kk+2,1)+qyt*he
2/12;
```

```
kk=kk+3;fs(kk,1)=fs(kk,1)+qx*kats3;fs(kk+1,1)=fs(kk+1,1)+qy*kats3;fs(kk+2,1)=fs(kk+2,1
)+qyt*he2/12;
end
re=l3;aex=abx-re*ww3^2*c3-re*aal3*s3;aby=-re*ww3^2*s3+re*aal3*c3;
fs(kk,1)=fs(kk,1)-m3*aex;fs(kk+1,1)=fs(kk+1,1)-m3*aey;fs(kk+2,1)=fs(kk+2,1)-ig3*aal3;
%---Newmark integration
alpha=0.25*(1+gama)^2;delta=0.5+gama;
a0=1/(alpha*dt^2);a1=delta/(alpha*dt);
a2=1/(alpha*dt);a3=1/(2*alpha)-1;
a4=delta/alpha-1;a5=(dt/2)*(delta/alpha-2);
a6=dt*(1-delta);a7=delta*dt;
t=0:dt:tson;ns=length(t);
u(1:nb,1:ns)=0;u1(1:nb,1:ns)=0;u2(1:nb,1:ns)=0;
  ti=t(ni);
  thm=thm2;w0=wmax2;velti;th2=fis2+th;w2=w;al2=al;
  thm=thm3;w0=wmax3;velti;th3=th2+fis3+th;w3=w2+w;al3=al2+al;
  c2=cos(th2);s2=sin(th2);c3=cos(th3);s3=sin(th3);
  ;mat1=a0*ms+a1*cs+ks;mat1=inv(mat1)
  up=u(1:nb,ni-1);u1p=u1(1:nb,ni-1);u2p=u2(1:nb,ni-1);
  uc=fs+ms*(a0*up+a2*u1p+a3*u2p)+cs*(a1*up+a4*u1p+a5*u2p);uc=mat1*uc;
  u2c=a0*(uc-up)-a2*u1p-a3*u2p;
  u1c=u1p+a6*u2p+a7*u2c;
  u(1:nb,ni)=uc;u1(1:nb,ni)=u1c;u2(1:nb,ni)=u2c;
end
nf=nf2;
ux=u(nf,1:ns);uy=u(nf+1,1:ns);usum=sqrt(ux.^2+uy.^2); %displacement (m)
ux1=u1(nf,1:ns);uy1=u1(nf+1,1:ns); %velocity
ux2=u2(nf,1:ns);uy2=u2(nf+1,1:ns); %acceleration

fi=fis2+thm2+fis3+thm3+pi/2;c=cos(fi);s=sin(fi);
ud=ux*c+uy*s;ud1=ux1*c+uy1*s;ud2=ux2*c+uy2*s;
%plot(t,uy)  % y-axes deflection (m); pause
%axis([0 tson -10 10]),hold on,plot(t,ud2),xlabel('time (s)'),ylabel('acceleration
(m/s^2'),legend('Linearly tapered function')
```

```
ns1=round(tmotion/dt);ns2=round(tson/dt);
t1=t(ns1:ns2);y1=ud2(ns1:ns2);
yrms=sqrt(mean(y1.^2)),
figure (1),
acc_scale=10;
hold on;subplot(2,1,1);axis([0 tson -acc_scale acc_scale]);hold
on;p1=plot(t,ud2);set(p1,'Color','red','LineWidth',2);xlabel('(tm=2s and tres=5s)    Time
(s)');ylabel('Acceleration (m/s^2)'),title('Simulation Case Results for Sy1-varying-al2'),
legend('Case: SR-ta-t1h-t1h-2');
hold on;subplot(2,1,2);axis([0 tson -acc_scale acc_scale]);hold
on;p2=plot(t1,y1);set(p2,'Color','black','LineWidth',2);legend('residual vibration
data'),xlabel('(tres=5s for residual vibration)   Time (s)');ylabel('Acceleration (m/s^2)');
```